Article

Neuron

Basolateral to Central Amygdala Neural Circuits for Appetitive Behaviors

Highlights

- Several genetically distinct CeA neurons mediate appetitive behaviors
- BLA *Ppp1r1b*$^{+}$ neurons project to CeA neurons that mediate appetitive behaviors
- BLA *Rspo2*$^{+}$ neurons project to CeA neurons that suppress appetitive behaviors
- BLA-to-CeA pathways are analogous to corticostriatal direct and indirect pathways

Authors

Joshua Kim, Xiangyu Zhang, Shruti Muralidhar, Sarah A. LeBlanc, Susumu Tonegawa

Correspondence

joshuak@mit.edu (J.K.), tonegawa@mit.edu (S.T.)

In Brief

Kim and Zhang et al. dissect genetically defined circuits for appetitive behaviors from the basolateral amygdala to the central amygdala that are genetically analogous to the direct and indirect pathways of the cortex and striatum.

Kim et al., 2017, Neuron *93*, 1464–1479
March 22, 2017
http://dx.doi.org/10.1016/j.neuron.2017.02.034

CellPress

CellPress

Neuron
Article

Basolateral to Central Amygdala Neural Circuits for Appetitive Behaviors

Joshua Kim,[1,4,*] Xiangyu Zhang,[1,4] Shruti Muralidhar,[1] Sarah A. LeBlanc,[1] and Susumu Tonegawa[1,2,3,5,*]
[1]RIKEN-MIT Center for Neural Circuit Genetics at The Picower Institute for Learning and Memory, Department of Biology and Department of Brain and Cognitive Sciences, Massachusetts Institute of Technology, Cambridge, MA 02139, USA
[2]Howard Hughes Medical Institute, Massachusetts Institute of Technology, Cambridge, MA 02139, USA
[3]Brain Science Institute, RIKEN, Saitama 351-0198, Japan
[4]Co-first author
[5]Lead Contact
*Correspondence: joshuak@mit.edu (J.K.), tonegawa@mit.edu (S.T.)
http://dx.doi.org/10.1016/j.neuron.2017.02.034

SUMMARY

Basolateral amygdala (BLA) principal cells are capable of driving and antagonizing behaviors of opposing valence. BLA neurons project to the central amygdala (CeA), which also participates in negative and positive behaviors. However, the CeA has primarily been studied as the site for negative behaviors, and the causal role for CeA circuits underlying appetitive behaviors is poorly understood. Here, we identify several genetically distinct populations of CeA neurons that mediate appetitive behaviors and dissect the BLA-to-CeA circuit for appetitive behaviors. Protein phosphatase 1 regulatory subunit 1B$^+$ BLA pyramidal neurons to dopamine receptor 1$^+$ CeA neurons define a pathway for promoting appetitive behaviors, while R-spondin 2$^+$ BLA pyramidal neurons to dopamine receptor 2$^+$ CeA neurons define a pathway for suppressing appetitive behaviors. These data reveal genetically defined neural circuits in the amygdala that promote and suppress appetitive behaviors analogous to the direct and indirect pathways of the basal ganglia.

INTRODUCTION

The basolateral amygdala (BLA) and central amygdala (CeA) are involved in the control of emotional behaviors (Gallagher and Chiba, 1996; Swanson and Petrovich, 1998). The BLA contains two spatially segregated, genetically distinct populations of cortical-like excitatory pyramidal neurons: protein phosphatase 1 regulatory subunit 1B$^+$ (*Ppp1r1b*$^+$, also known as DARPP-32) parvocellular neurons and R-spondin 2$^+$ (*Rspo2*$^+$) magnocellular neurons (Carlsen and Heimer, 1988; Hemmings et al., 1984; Kim et al., 2016; McDonald, 1984; Pitkänen et al., 1997; Swanson and Petrovich, 1998). BLA *Ppp1r1b*$^+$ neurons elicit appetitive behaviors, inhibit defensive behaviors, and send projections to the lateral nucleus of the CeA (CeL) and the medial nucleus of the CeA (CeM). BLA *Rspo2*$^+$ neurons elicit defensive behaviors, inhibit appetitive behaviors, and send projections to the capsular nucleus of the CeA (CeC) (Kim et al., 2016). The CeA consists of GABAergic striatal medium spiny-like neurons and, similar to the BLA, is critical for appetitive and defensive behaviors (Gallagher and Chiba, 1996; McDonald, 1991; Swanson and Petrovich, 1998).

The CeA has been mainly studied on the basis of its role in innate and learned fear-related behaviors (Davis, 1992; Duvarci and Pare, 2014; Ehrlich et al., 2009; Goosens and Maren, 2001; Herry and Johansen, 2014; Hitchcock and Davis, 1986; Killcross et al., 1997; LeDoux et al., 1988). Cell-type-specific studies have shown evidence for the involvement of several genetically defined CeA neurons in aversive behaviors such as defensive responses and anxiogenesis (Andero et al., 2014; Han et al., 2015; Haubensak et al., 2010; Isosaka et al., 2015; Li et al., 2013; McCall et al., 2015; Pomrenze et al., 2015; Sanford et al., 2017). However, despite early evidence suggesting the involvement of the CeA in appetitive behaviors (Galaverna et al., 1993; Gallagher et al., 1990; Parkinson et al., 2000; Ritter and Hutton, 1995) and more recent activation studies demonstrating a modulatory role of the CeA in appetitive behaviors (Cai et al., 2014; Robinson et al., 2014; Seo et al., 2016), how appetitive behavior integrates into a structural and functional model of amygdala has yet to be established. For instance, a genetically defined population of CeA neurons that are positive mediators of appetitive behavior has not been identified. Given the strong projections from BLA *Ppp1r1b*$^+$ parvocellular neurons to the CeL and CeM (Kim et al., 2016), we hypothesized that the CeA may contain neurons that are positive mediators of appetitive behavior. Therefore, we first examined the role of genetically distinct CeA populations in both appetitive and defensive behaviors. Furthermore, although the BLA and CeA are both important for appetitive and defensive behaviors, it is not known how BLA *Ppp1r1b*$^+$ parvocellular and BLA *Rspo2*$^+$ magnocellular neurons are connected to genetically defined CeA neurons. Therefore, we also examined the connectivity from genetically defined neurons from the BLA to the CeA. Lastly, cytoarchitectural studies suggest that the BLA and CeA are structurally similar to the cortex and striatum, respectively (Carlsen and Heimer, 1988; Swanson and Petrovich, 1998). For this reason, we explored the expression pattern of striatal markers in the CeA to examine whether there exists an organizing principle in the BLA-to-CeA circuit that is common with the cortex and striatum.

RESULTS

Prkcd, *Nts*, *Sst*, and *Tac2* Define Distinct Cellular Populations in the CeA

Gene expression studies have shown a wide range of genetic diversity within the CeA (Cornea-Hébert et al., 1999; Moga and Gray, 1985; Skofitsch and Jacobowitz, 1985; Warden and Young, 1988; Zirlinger et al., 2001). To identify genetically distinct populations in the CeA, we performed single-molecule fluorescence in situ hybridization (smFISH) (ACDBio RNAscope) of genes that are expressed in the CeA—calcitonin receptor-like (*Calcrl*), corticotropin-releasing hormone (*Crh*), serotonin receptor 2a (*Htr2a*), neurotensin (*Nts*), protein kinase C-δ (*Prkcd*), somatostatin (*Sst*), and tachykinin 2 (*Tac2*). It should be noted that, for the CeC, only the anterior region was quantified due to the ambiguity of the CeC in the posterior CeA (Figure S1B). *Calcrl* and *Prkcd* were expressed in the CeC; *Crh*, *Htr2a*, *Nts*, *Prkcd*, *Sst*, and *Tac2* were expressed in the CeL; and *Htr2a*, *Nts*, *Sst*, and *Tac2* were expressed in the CeM (Figures S1A and S1B). Overlap of the expression of *Calcrl*, *Crh*, *Nts*, *Prkcd*, *Sst*, and *Tac2* was examined in the CeA. In the CeC, *Calcrl* labeled 89% of *Prkcd*$^+$ neurons, while *Prkcd* labeled 56% of *Calcrl*$^+$ neurons (Figures 1A and 1D). *Calcrl*$^+$ neurons were non-overlapping with *Sst* (which delineates the CeL) in the CeA (Figure 1I), further indicating that *Calcrl*$^+$ neurons reside in the CeC rather than the CeL. In the CeL, several of the genes had significantly high levels of overlap (>50%) (Figures 1B and 1J–1O). Using the levels of overlap among pairs of genes, hierarchical clustering revealed three major clusters: the first containing *Prkcd*; the second containing *Sst*; and third containing *Crh*, *Tac2*, and *Nts* (Figure 1B). In the CeM, *Crh*, *Nts*, *Sst*, and *Tac2* were minimally (<15%) overlapping (Figure 1C). *Htr2a* expression was weak and difficult to quantify with a high degree of confidence in the CeA. However, based upon a few double-label smFISHs, several *Htr2a*$^+$ neurons were found to coexpress *Crh*, *Prkcd*, *Nts*, *Sst*, and *Tac2* in the CeL and *Nts*, *Sst*, and *Tac2* in the CeM (Figure S1D). Therefore, *Htr2a* may be less specific for labeling a distinct population compared to the other genes. Collectively, characterization using these sets of genes revealed as many as eight or nine genetically and regionally distinguishable populations of neurons in the CeA.

For this study, we have chosen to study seven major neuronal populations of the CeA, distinguishable based on gene expression and region—CeC *Prkcd*$^+$, CeL *Prkcd*$^+$, CeL *Crh*$^+$*Nts*$^+$*Tac2*$^+$, CeL *Sst*$^+$, CeM *Nts*$^+$, CeM *Sst*$^+$, and CeM *Tac2*$^+$ (Figure 1P). To determine the proportion of neurons that CeL *Prkcd*$^+$, CeL *Crh*$^+$*Nts*$^+$*Tac2*$^+$, and CeL *Sst*$^+$ neurons constitute in the CeL and the proportion of neurons that CeM *Nts*$^+$, CeM *Sst*$^+$, and CeM *Tac2*$^+$ neurons constitute in the CeM, the expression of *Nts*, *Prkcd*, *Sst*, and *Tac2* with glutamate decarboxylase 1 (*Gad1*), a marker of inhibitory neurons, was examined. *Prkcd*, *Sst*, and *Tac2* collectively labeled 96% of *Gad1*$^+$ neurons in the CeL, whereas *Prkcd*$^+$, *Sst*$^+$, and *Tac2*$^+$ neurons were 100% *Gad1*$^+$ (Figure S1C). *Nts*, *Sst*, and *Tac2* collectively labeled 95% of *Gad1*$^+$ neurons in the CeM, whereas *Nts*$^+$, *Sst*$^+$, and *Tac2*$^+$ were 100% *Gad1*$^+$ (Figure S1C). This suggests that CeL *Prkcd*$^+$, CeL *Crh*$^+$*Nts*$^+$*Tac2*$^+$, and CeL *Sst*$^+$ neurons constitute the majority of GABAergic neurons in the CeL and that CeM *Nts*$^+$, CeM *Sst*$^+$, and CeM *Tac2*$^+$ neurons constitute the majority of GABAergic neurons in the CeM.

Genetically Distinct CeA Populations that Drive Appetitive and Defensive Behaviors

The CeA has been shown to participate in defensive behaviors and appetitive behaviors (Galaverna et al., 1993; Gallagher et al., 1990; Goosens and Maren, 2001; Killcross et al., 1997; LeDoux et al., 1988; Parkinson et al., 2000). Therefore, each of the seven CeA neuronal populations was subjected to optogenetic stimulation experiments to assess these functions. CeC *Prkcd*$^+$ and CeL *Prkcd*$^+$ neurons were targeted using a Cre-dependent channelrhodopsin (ChR2) virus injected into the CeC and CeL, respectively, of the *Prkcd*-Cre mice; CeL *Sst*$^+$ and CeM *Sst*$^+$ neurons were targeted using injections into the CeL and CeM, respectively, of the *Sst*-Cre mice; CeL *Crh*$^+$*Nts*$^+$*Tac2*$^+$ neurons were targeted using injections into the CeL of *Crh*-Cre mice; CeM *Nts*$^+$ neurons were targeted using injections into the CeM of *Nts*-Cre mice; and CeM *Tac2*$^+$ neurons were targeted using injections into the CeM of the *Tac2*-Cre mice (Figure S2A). Control mice were Cre$^-$ mice that underwent identical surgical procedures in the CeC (*Prkcd*-Cre$^-$ mice), CeL (*Sst*-Cre$^-$ mice), and CeM (*Tac2*-Cre$^-$ mice). In the optogenetic freezing test, mice were placed into a neutral conditioning chamber, where no light stimulation occurred during the 0- to 3-min period (OFF), followed by 20-Hz blue-light stimulation during the 3- to 6-min period (ON). Stimulation of CeC *Prkcd*$^+$ neurons elicited freezing (Figure 2A), measured by an increase in freezing during the ON period compared to the OFF period, while stimulation of CeL *Prkcd*$^+$, CeL *Crh*$^+$*Nts*$^+$*Tac2*$^+$, CeL *Sst*$^+$, CeM *Nts*$^+$, CeM *Sst*$^+$, and CeM *Tac2*$^+$ neurons did not elicit freezing (Figures 2B–2G). It should be noted, that stimulation of CeM *Tac2*$^+$ neurons elicited immobility-like behaviors but did not reflect stereotypical freezing. Rather, this immobility-like behavior due to activation of CeM *Tac2*$^+$ neurons coincided with biting behavior in five out of eight mice. Cre$^-$ control mice did not demonstrate light-induced freezing (Figure S2B). Following the freezing test, mice were tested for self-stimulation. In the optogenetic self-stimulation test, mice were freely allowed to poke into two nose ports for a single session of 60 min, where only one port delivered 20-Hz blue-light stimulation. Activation of CeL *Sst*$^+$, CeL *Crh*$^+$*Nts*$^+$*Tac2*$^+$, CeM *Nts*$^+$, CeM *Sst*$^+$, and CeM *Tac2*$^+$ neurons resulted in self-stimulation, based on an increased in nose pokes in the light-stimulated port (ON) compared to the unstimulated port (OFF) (Figures 2C–2G), while CeC *Prkcd*$^+$ and CeL *Prkcd*$^+$ neurons did not result in self-stimulation (Figures 2A and 2B). Cre$^-$ control mice did not demonstrate light-induced self-stimulation (Figure S2B). These optogenetic stimulation experiments demonstrate that CeL *Sst*$^+$, CeL *Crh*$^+$*Nts*$^+$*Tac2*$^+$, CeM *Nts*$^+$, CeM *Sst*$^+$, and CeM *Tac2*$^+$ neurons are capable of driving appetitive behaviors, CeC *Prkcd*$^+$ neurons are capable of driving defensive behaviors, while CeL *Prkcd*$^+$ neurons are not capable of driving either appetitive or defensive behaviors.

Appetitive and Threatening Stimuli Activate Distinct CeA Populations

Distinct CeA neurons are capable of eliciting defensive behaviors and appetitive behaviors. Therefore, to assess how these

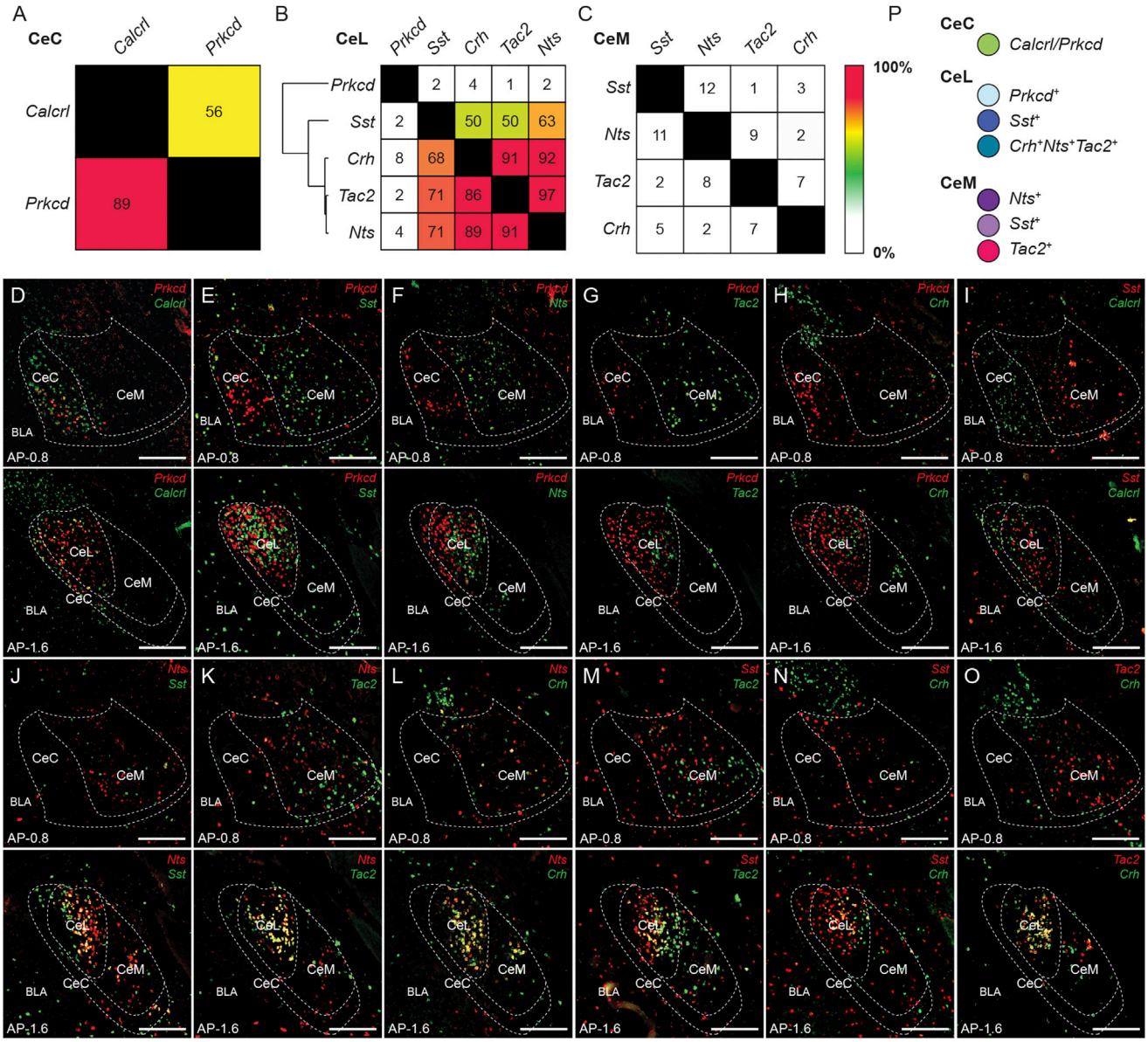

Figure 1. Identification of Genetically Distinct Populations in the CeA

(A–C) Quantification of overlap of *Prkcd* and *Calcrl* in the CeC (A). Quantification of overlap of *Prkcd*, *Sst*, *Crh*, *Tac2*, and *Nts* in the CeL (B). Quantification of overlap of *Sst*, *Nts*, *Tac2*, and *Crh* in the CeM (C). Values represent percent labeling of overlap of genes in column among genes in rows. For example, 56% of CeC *Calcrl* neurons coexpress *Prkcd* (A). Values represent percentage of labeling from totaling all cells counted from n = 3 mice. Hierarchical clustering was performed in the CeL using the percent overlap profile of each gene (B).

(D–O) Representative histology of CeA expression of *Prkcd* and *Calcrl* (D), *Prkcd* and *Sst* (E), *Prkcd* and *Nts* (F), *Prkcd* and *Tac2* (G), *Prkcd* and *Crh* (H), *Sst* and *Calcrl* (I), *Nts* and *Sst* (J), *Nts* and *Tac2* (K), *Nts* and *Crh* (L), *Sst* and *Tac2* (M), *Sst* and *Crh* (N), and *Tac2* and *Crh* (O) in the anterior CeA (anterior-posterior [AP] distance from bregma, −0.8 mm) and posterior CeA (AP distance from bregma, −1.6 mm). Scale bars, 250 μm.

(P) Seven major populations of neurons that were selected for examination and color selection for subsequent data presentation; CeC *Prkcd*$^+$ (green), CeL *Prkcd*$^+$ (light blue), CeL *Sst*$^+$ (dark blue), CeL *Crh*$^+$*Nts*$^+$*Tac2*$^+$ (teal), CeM *Sst*$^+$ (light purple), CeM *Nts*$^+$ (dark purple), and CeM *Tac2*$^+$ (magenta) neurons.

populations are activated by external stimuli, the expression of the activity-dependent gene, *Fos* (Dubner and Ruda, 1992), was measured in each of the seven CeA neuronal populations in response to five different conditions associated with defensive or appetitive behaviors. Wild-type mice were exposed to either footshocks or no footshocks; contextual fear extinction recall or contextual fear recall without fear extinction; ad libitum food or no food in food-deprived mice; ad libitum water, quinine water, or no water in water-deprived mice; and injection of cholecystokinin (CCK, an agent that induces satiety) or saline in mice 30 min prior to sacrifice (see STAR Methods). The percentages of *Fos* labeling within each of the CeA populations were

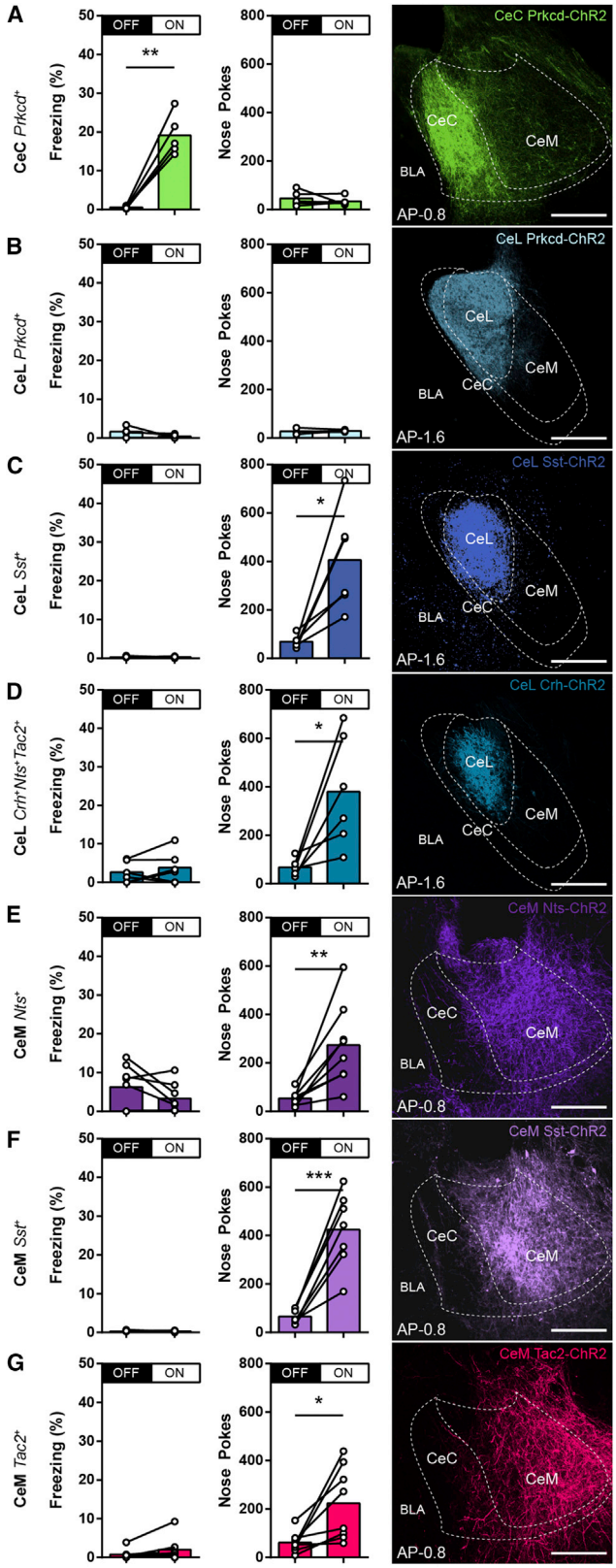

Figure 2. Genetically Distinct CeA Neurons Drive Appetitive and Defensive Behaviors

(A–G) Behavioral assessment of percent freezing without (OFF) or with (ON) photostimulation (first column) and total number of nose pokes in unstimulated (OFF) or photostimulated (ON) port in self-stimulation experiments (second column) from optogenetic activation of CeC *Prkcd*$^+$ (n = 5) (A), CeL *Prkcd*$^+$ (n = 4) (B), CeL *Sst*$^+$ (n = 6) (C), CeL *Crh*$^+$*Nts*$^+$*Tac2*$^+$ (n = 6) (D), CeM *Nts*$^+$ (n = 7) (E), CeM *Sst*$^+$ (n = 7) (F), and CeM *Tac2*$^+$ (n = 8) (G) neurons. Representative histology of ChR2 expression in the targeted CeA neurons (third column). Anterior-posterior distribution of the ChR2 expression found in Figure S2A. All animals underwent the optogenetic freezing test, followed by the optogenetic self-stimulation test. ChR2 expression was pseudocolored in correspondence with selected color scheme (Figure 1P). Significance for paired t test: *$p < 0.05$; **$p < 0.01$; ***$p < 0.001$. AP distance from bregma is given (in millimeters). Scale bars, 250 μm.

See also Figure S2A.

measured. *Fos* expression was increased in CeC *Prkcd*$^+$ neurons in response to footshocks, compared to corresponding control (Figure 3A), and in response to contextual fear recall compared to contextual fear extinction recall (Figure 3B). *Fos* expression was also measured in CeC *Calcrl*$^+$ neurons in response to footshocks and was found to be significantly increased in CeC *Calcrl*$^+$ neurons (Figure S3B). This is consistent with the observation that CeC *Prkcd* labels a subpopulation of CeC *Calcrl*$^+$ neurons (Figure 1A). *Fos* expression was increased in CeL *Prkcd*$^+$ neurons in response to contextual fear extinction recall compared to contextual fear recall (Figure 3B). *Fos* expression was increased in CeL *Prkcd*$^+$, CeL *Sst*$^+$, CeL *Crh*$^+$*Nts*$^+$*Tac2*$^+$, CeM *Nts*$^+$, CeM *Sst*$^+$, and CeM *Tac2*$^+$ neurons in response to ad libitum food and ad libitum water compared to corresponding controls (Figures 3C and 3D). *Fos* expression was increased in CeL *Prkcd*$^+$ in response to CCK (Figure 3E). *Fos* expression was increased in CeC *Prkcd*$^+$ in response to quinine in water-deprived mice (Figure 3D). These results suggest that CeC *Prkcd*$^+$ neurons are activated by threatening stimuli and aversive tastes. CeL *Prkcd*$^+$ neurons are activated by states of suppression of defensive behaviors and stimuli that suppress appetitive behaviors. CeL *Sst*$^+$, CeL *Crh*$^+$*Nts*$^+$*Tac2*$^+$, CeM *Nts*$^+$, CeM *Sst*$^+$, and CeM *Tac2*$^+$ neurons are activated by stimuli that elicit appetitive behaviors.

Silencing CeA Populations in Feeding, Drinking, and Freezing

Differential *Fos* expression in the CeA in response to food, water, and footshock suggests that there may be differential involvement of these seven CeA populations in feeding, drinking, and freezing behaviors. Therefore, to dissociate the contribution of distinct CeA populations in these behaviors, each of the seven CeA neuronal populations was subjected to a series of optogenetic inhibition experiments (see STAR Methods). For targeting these populations, a Cre-dependent archaerhodopsin (Arch) virus was injected in the same fashion as in the previous optogenetic stimulation experiments, while littermate Cre$^-$ mice that underwent identical procedures were used as controls. When presenting ad libitum food to food-deprived mice during a 10-min trial, inhibition of each of the CeA populations—CeC *Prkcd*$^+$, CeL *Prkcd*$^+$, CeL *Sst*$^+$, CeL *Crh*$^+$*Nts*$^+$*Tac2*$^+$, CeM *Nts*$^+$, CeM *Sst*$^+$, and CeM *Tac2*$^+$—did not result in any significant

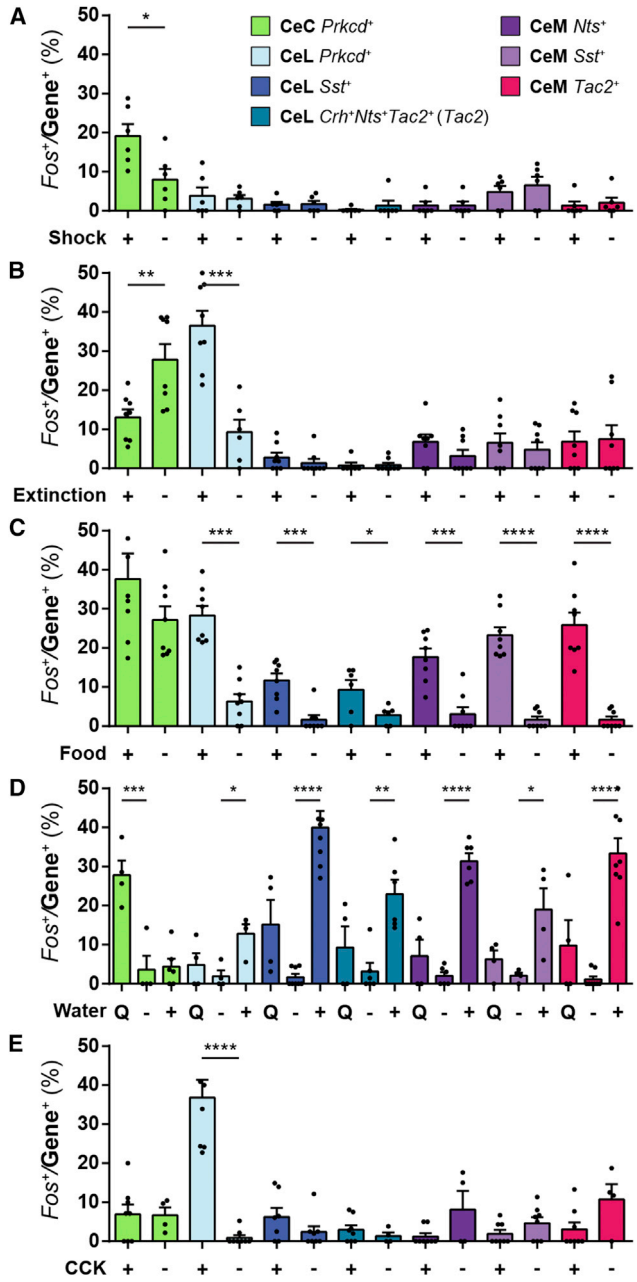

Figure 3. Genetically Distinct CeA Neurons Are Activated by Distinct Stimuli

(A–E) The percent overlap of *Fos* within CeC *Prkcd*$^+$, CeL *Prkcd*$^+$, CeL *Sst*$^+$, CeL *Crh*$^+$*Nts*$^+$*Tac2*$^+$, CeM *Nts*$^+$, CeM *Sst*$^+$, and CeM *Tac2*$^+$ neurons in response to shock (+) or no shock (-) (A); contextual fear extinction recall (+) or contextual fear recall (-) (B); ad libitum food (+) or no food (-) in food-deprived mice (C); quinine water (Q), no water (-), or ad libitum water (+) in water-deprived mice (D); and cholecystokinin (CCK) (+) or saline (-) injection (E). CeL *Crh*$^+$*Nts*$^+$*Tac2*$^+$ neurons were measured by quantifying *Fos* in *Tac2*$^+$ neurons in the CeL. Significance for unpaired t test (A), (B), (C), and (E) and one-way ANOVA with Bonferroni's multiple hypothesis correction comparing experimental groups with no water control (D): *p < 0.05; **p < 0.01; ***p < 0.001; ****p < 0.0001. Values are mean ± SEM from one to two sections per mouse from up to n = 4 mice. Individual values are indicated by black dots; some values that are too large and beyond the limit of the y axis are not shown.

changes in the duration of feeding behavior compared to corresponding controls (Figures 4A–4G). Subsequently, when presenting ad libitum water to water-deprived mice during a 5-min trial, inhibition of CeL *Prkcd*$^+$ neurons resulted in an increase in drinking behavior (Figure 4B), inhibition of CeL *Sst*$^+$ and CeL *Crh*$^+$*Nts*$^+$*Tac2*$^+$ resulted in a decrease in drinking behavior (Figures 4C and 4D), and inhibition of CeC *Prkcd*$^+$, CeM *Nts*$^+$, CeM *Sst*$^+$, and CeM *Tac2*$^+$ did not result in changes to drinking compared to corresponding controls (Figures 4A and 4E–4G). Finally, mice underwent contextual fear conditioning in which CeA neurons were inhibited during the presentation of three footshocks in a contextual fear conditioning protocol (day 1) and were subsequently reexposed to the conditioning chamber 24 hr later with no light inhibition (day 2). Inhibition of CeC *Prkcd*$^+$ neurons resulted in a minor, but statistically significant, reduction in freezing on day 1 and subsequently reduced levels of freezing on day 2 compared to corresponding controls (Figure 4A). Although there is a trend for increased freezing levels from inhibition of CeL *Prkcd*$^+$ neurons as previously reported (Haubensak et al., 2010), inhibition of the any of the CeA populations did not affect freezing on day 1 or 2 compared to corresponding controls (Figures 4B–4G). Together, these data suggest that CeL *Prkcd*$^+$ and CeL *Prkcd*$^-$ (CeL *Sst* and CeL *Crh*$^+$*Nts*$^+$*Tac2*$^+$) neurons have opposing roles on drinking and that CeC *Prkcd*$^+$ neurons are required for defensive behaviors, while inhibition of any one of these populations does not affect feeding behavior in food-deprived mice.

Inhibition of CeM *Nts*$^+$, CeM *Sst*$^+$, or CeM *Tac2*$^+$ neurons did not affect feeding, drinking or freezing behaviors. Therefore, the effects of collectively inhibiting all three CeM populations were assessed. CeM *Nts*$^+$, CeM *Sst*$^+$, and CeM *Tac2*$^+$ neurons collectively constitute almost all CeM *Drd1*$^+$ neurons (Figure S7E). Thus, a Cre-dependent Arch virus was injected into the CeM of *Drd1*-Cre mice and underwent the same procedures as the previous inhibition experiments (Figure 4). Inhibition of CeM *Drd1*$^+$ neurons resulted in the reduction of feeding behavior in food-deprived mice and the reduction of drinking in water-deprived mice, and no differences were shown in freezing in response to footshocks compared to corresponding controls (Figure S4). Therefore, CeM *Drd1*$^+$ neurons are critical for both feeding and drinking behavior and suggest that CeM *Nts*$^+$, CeM *Sst*$^+$, and CeM *Tac2*$^+$ neurons may collectively function to mediate feeding and drinking.

CeA Mediators of Appetitive Behavior Project to the Midbrain

The CeA is one of the output structures of the amygdala and is known to project to several brain regions, including the periaqueductal gray (PAG), and it has been widely hypothesized that PAG-projecting CeA neurons mediate freezing (Duvarci and Pare, 2014; Ehrlich et al., 2009; Herry and Johansen, 2014; Penzo et al., 2014). Therefore, the relationship between PAG-projecting CeA neurons and genetically distinct CeA populations was examined. The retrograde tracer, cholera toxin subunit B (CTB), was injected into the PAG. This resulted in CTB$^+$ neurons in the CeL and CeM that were *Sst*$^+$, *Tac2*$^+$, and *Nts*$^+$ (Figures S5A–S5C). In contrast, CTB retrograde tracing from the PAG did not label *Prkcd*$^+$ neurons in the CeL (Figures S5A–S5C), which is

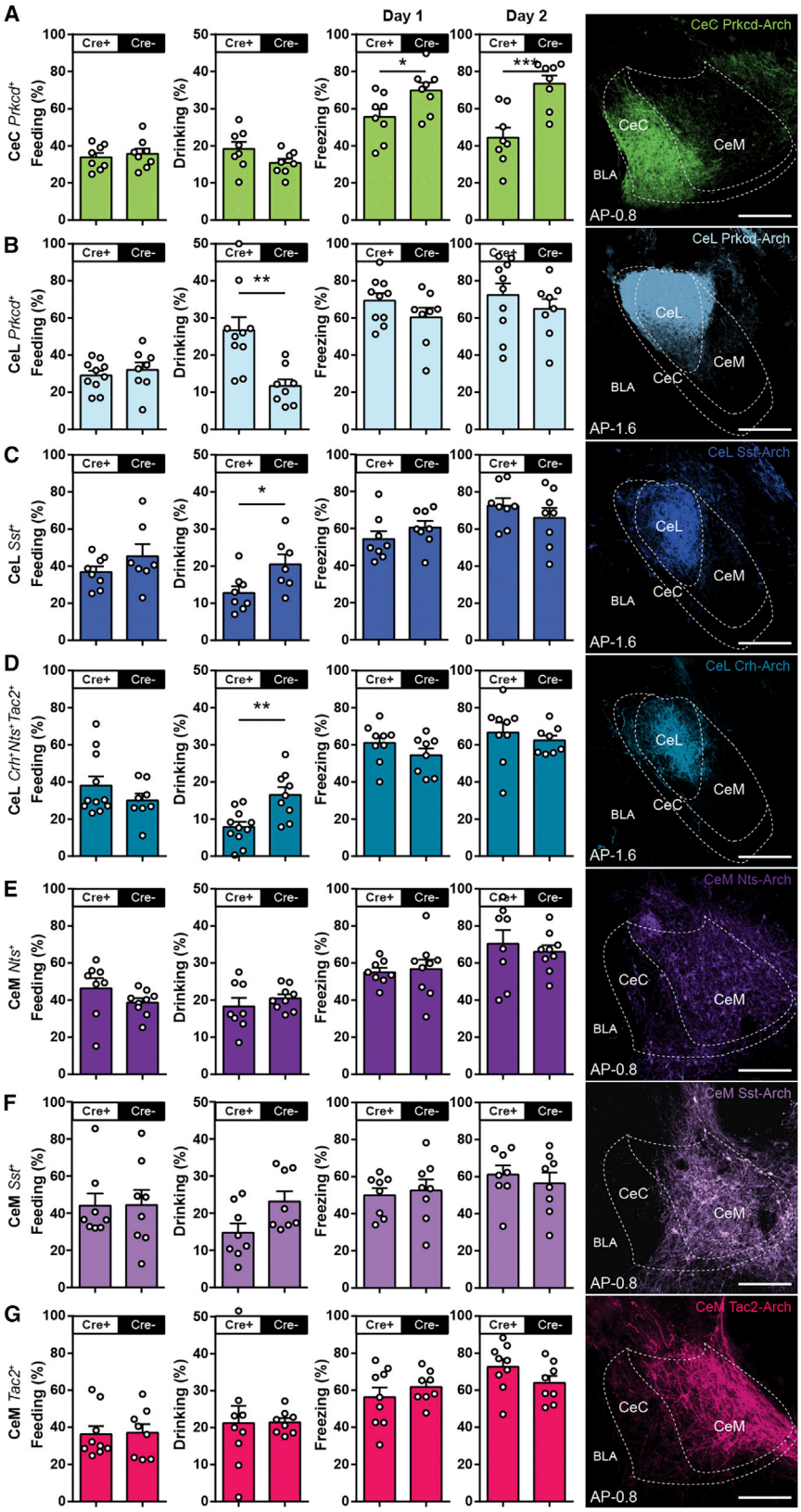

Figure 4. Inhibition of Genetically Defined CeA Neurons during Feeding, Drinking, and Defensive Behaviors

(A–G) Behavioral assessment of percent feeding during food presentation in food-deprived mice (first column), percent drinking during water presentation in water-deprived mice (second column), percent freezing during presentation of footshocks on day 1 (third column), and contextual recall without optogenetic inhibition on day 2 (fourth column) from optogenetic inhibition of CeC *Prkcd*$^+$ (n = 8, 8 [n = experimental, control]) (A), CeL *Prkcd*$^+$ (n = 10, 8) (B), CeL *Sst*$^+$ (n = 8, 8) (C), CeL *Crh*$^+$*Nts*$^+$*Tac2*$^+$ (n = 8, 8) (D), CeM *Nts*$^+$ (n = 9, 8) (E), CeM *Sst*$^+$ (n = 8, 8) (F), and CeM *Tac2*$^+$ (n = 9, 8) (G) neurons. All animals underwent the feeding test, followed by the drinking test, which was then followed by contextual fear conditioning. Representative histology of eArch3.0 expression and optic fiber placement in the targeted CeA neurons (fifth column). eArch3.0 expression was pseudocolored in correspondence with selected color scheme (Figure 1P). Significance for unpaired t test: *p < 0.05; **p < 0.01; ***p < 0.001. AP distance from bregma is given (in millimeters). Scale bars, 250 μm.

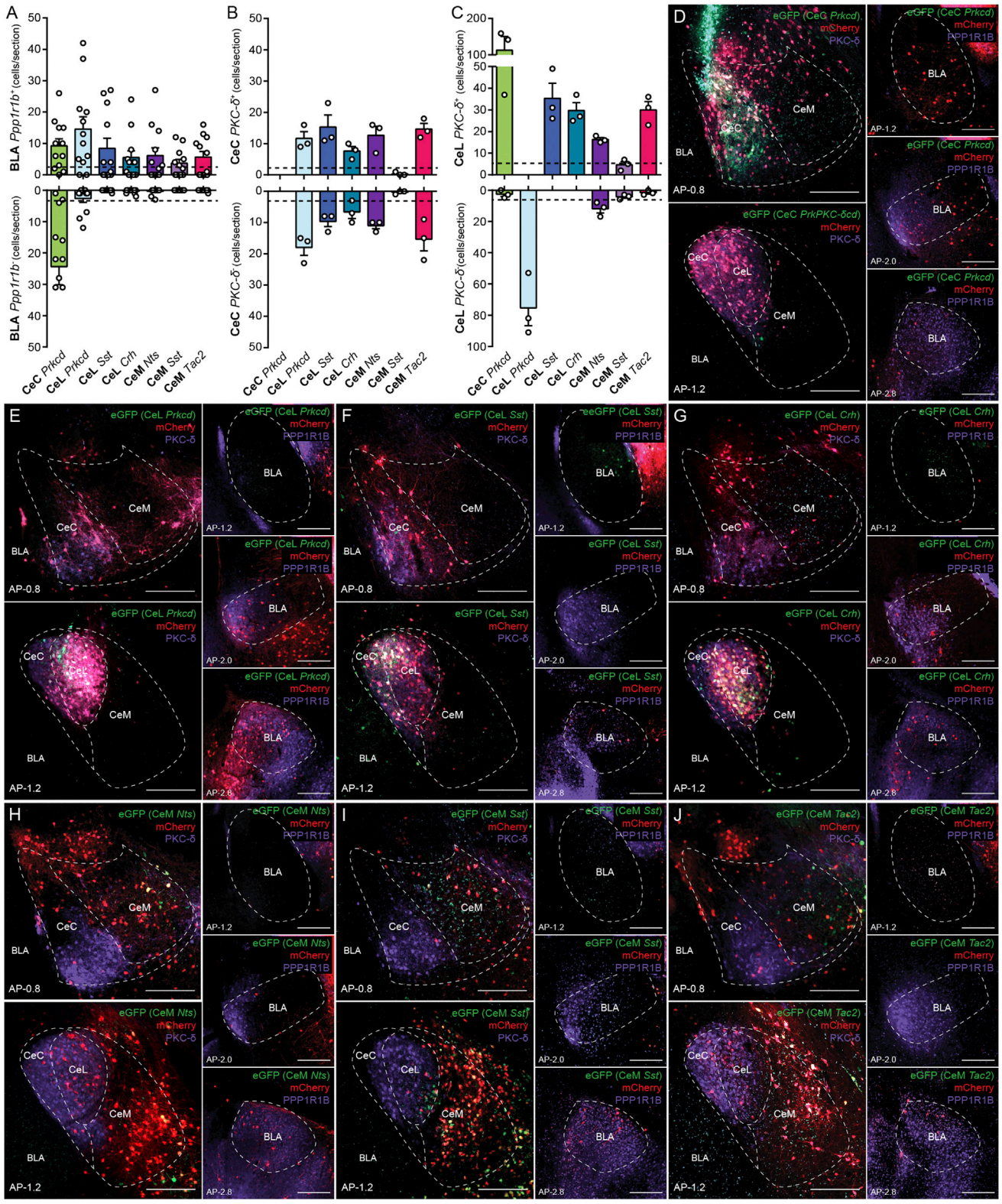

(legend on next page)

consistent with previous reports (Penzo et al., 2014). Using ChR2 mice (Figure 2), anterograde tracing fibers were found in the PAG of CeL-Sst-ChR2, CeL-Crh-ChR2, CeM-Nts-ChR2, CeM-Sst-ChR2, and CeM-Tac2-ChR2 mice, but not CeC-Prkcd-ChR2 and CeL-Prkcd-ChR2 mice (Figure S5D). These data suggest that CeL *Sst*$^+$, CeL *Crh*$^+$*Nts*$^+$*Tac2*$^+$, CeM *Nts*$^+$, CeM *Sst*$^+$, and CeM *Tac2*$^+$ neurons project to the PAG, while CeC *Prkcd*$^+$ and CeL *Prkcd*$^+$ neurons do not project the PAG. These findings suggest that, independent of whether appetitive functions are necessarily mediated by transmission from the CeA to the PAG, PAG projections may not be a unique structural feature of CeA neurons that mediate defensive function.

BLA *Ppp1r1b*$^+$ Neurons Form Monosynaptic, while BLA *Rspo2*$^+$ Neurons Form Disynaptic Connections to CeA Mediators of Appetitive Behavior

Genetically defined BLA pyramidal neurons that are capable of driving defensive and appetitive behaviors send projections to the CeA (Kim et al., 2016). Therefore, the anatomical relationship between the BLA and CeA was examined using cell-type-specific monosynaptic rabies tracing in the seven CeA neuronal populations (Kohara et al., 2014; Wickersham et al., 2007). To target these populations, AAV (adeno-associated virus) helper virus, AAV_1-synP-FLEX-sTpEpB (Kohara et al., 2014; a construct containing Cre-dependent TVA [tumor virus A], rabies G protein, and EGFP) was injected in the same fashion as in the optogenetic stimulation experiments, incubated for 3 weeks prior to injection of the G-deleted rabies mCherry virus (Kohara et al., 2014), and then sacrificed 1 week later. Tissues were labeled using antibodies against PPP1R1B to determine the BLA cell type—*Ppp1r1b*$^+$ or *Ppp1r1b*$^-$ (as a measure of *Rspo2*$^+$ neurons because *Rspo2*$^+$ and *Ppp1r1b*$^+$ constitute virtually all BLA excitatory neurons) (Kim et al., 2016; Figures 5D–5J). Monosynaptic tracing from CeL *Prkcd*, CeL *Sst*$^+$, CeL *Crh*$^+$*Nts*$^+$*Tac2*$^+$, CeM *Nts*$^+$, CeM *Sst*$^+$, and CeM *Tac2*$^+$ neurons resulted in retrograde-labeled neurons in the BLA that are predominantly PPP1R1B$^+$ (Figure 5A). In contrast, monosynaptic tracing from CeC *Prkcd*$^+$ neurons resulted in retrograde-labeled neurons in the BLA that were PPP1R1B$^-$ but also PPP1R1B$^+$ (Figure 5A). These results suggest that BLA *Rspo2*$^+$ neurons directly project to CeC *Prkcd*$^+$ neurons, while BLA *Ppp1r1b*$^+$ neurons directly project to all CeA neurons that were examined. It should be noted that the connectivity from BLA *Ppp1r1b*$^+$ neurons to CeC neurons was not observed in our previous study (Kim et al., 2016). This apparent contradiction may be explained by the fact that we previously targeted the dorsal portion of the CeC for retrograde labeling, whereas CeC *Prkcd*$^+$ neurons reside more ventrally in the CeC (Figure S1B).

Monosynaptic tracing experiments were further analyzed using an antibody against protein kinase C δ (PKC-δ) for determining the retrograde-labeled CeA cell type (*Prkcd*$^+$ or *Prckd*$^-$). Monosynaptic tracing from CeL *Prkcd*, CeL *Sst*$^+$, CeL *Crh*$^+$*Nts*$^+$*Tac2*$^+$, CeM *Nts*$^+$, and CeM *Tac2*$^+$ neurons resulted in several (more than five neurons per section) retrograde-labeled neurons in the CeC that were PKC-δ$^+$ and PKC-δ$^-$ (Figure 5B). Monosynaptic tracing from CeC *Prkcd*, CeL *Sst*$^+$, CeL *Crh*$^+$*Nts*$^+$*Tac2*$^+$, CeM *Nts*$^+$, and CeM *Tac2*$^+$ neurons resulted in several (more than five neurons per section) retrograde-labeled neurons in the CeL that were PKC-δ$^+$ neurons (Figure 5C). Monosynaptic tracing from CeM *Nts*$^+$ neurons resulted in several (more than five neurons per section) retrograde-labeled neurons in the CeL that were PKC-δ$^-$ neurons (Figure 5C). Although no leaky viral expression was found (Figure S5E), due to possibilities of differential tropism across mouse lines, nonspecific targeting (Figure S5F), and unmeasurable leakiness, there may be more or less connectivity than demonstrated by these rabies experiments. Nevertheless, using an arbitrary threshold for retrograde labeling (>2.5 neurons per section in the BLA and more than five neurons per section in the CeA), a model of the BLA to CeA connectivity was generated (Figure 8A). Overall, these results demonstrate monosynaptic connections from BLA *Ppp1r1b*$^+$ neurons to the CeA neurons that mediate appetitive behaviors and a monosynaptic connection from BLA *Rspo2*$^+$ neurons primarily to CeC neurons that inhibit several of the CeA neuron populations that are capable of eliciting appetitive behavior.

The BLA-to-CeA connectivity was further assessed using slice patch-clamp recordings in conjunction with cell-type-specific optogenetic stimulation of the BLA. Cre-dependent ChR2 virus was injected into the BLA of *Rspo2*-Cre and *Cartpt*-Cre mice for targeting BLA *Rspo2*$^+$ (*Rspo2*-ChR2) and BLA *Ppp1r1b*$^+$ (*Ppp1r1b*-ChR2) neurons, respectively (Kim et al., 2016). Patch-clamped CeA neurons were recorded in response to ChR2 stimulation and were genetically identified using biocytin filling followed by immunohistochemistry against PKC-δ in the CeL or cytosolic harvesting followed by qPCR in the CeC and CeM. The electrical properties of these neurons were also measured (Figures S6A–S6D). Blue-light stimulation in *Ppp1r1b*-ChR2 slices resulted in monosynaptic excitation,

Figure 5. Monosynaptic Retrograde Tracing from Genetically Defined CeA Neurons

(A) Quantification of rabies-mediated retrograde-labeled PPP1R1B$^+$ and PPP1R1B$^-$ neurons in the BLA from genetically defined CeA neurons. Individual points represent the number of retrograde-labeled neurons per section in the BLA from n = 8 sections per mouse from n = 3 mice. Scale bars represent mean ± SEM. An arbitrary threshold of 2.5 neurons per section was used to construct a connectivity model (Figure 8A).

(B) Quantification of rabies-mediated retrograde-labeled PKC-δ$^+$ and PKC-δ$^-$ neurons in the CeC from genetically defined CeA neurons. Individual points represent the number of retrograde-labeled neurons per single section in the CeC from n = 3 sections from three mice. Scale bars, mean ± SEM. An arbitrary threshold of 2.5 neurons per section was used to construct a connectivity model (Figure 8A).

(C) Quantification of rabies-mediated retrograde-labeled PKC-δ$^+$ and PKC-δ$^-$ neurons in the CeL from genetically defined CeA neurons. Individual points represent the number of retrograde- labeled neurons per single section in the CeL from n = 3 sections from three mice. Scale bars, mean ± SEM. An arbitrary threshold of five neurons per section was used to construct a connectivity model (Figure 8A).

(D–J) Representative histology of rabies-mediated retrograde tracing from CeC *Prkcd*$^+$ neurons (D), CeL *Prkcd*$^+$ neurons (E), CeL *Sst*$^+$ neurons (F), CeL *Crh*$^+$*Nts*$^+$*Tac2*$^+$ neurons (G), CeM *Nts*$^+$ neurons (H), CeM *Sst*$^+$ neurons (I), and CeM *Tac2*$^+$ neurons (J) in the CeA and BLA. Starter cells are labeled with EGFP (green) and mCherry (red), and mouse line of starter cells are noted (italicized), Rabies virus is labeled with mCherry (red). Prkcd protein (purple) was labeled in the CeA. Ppp1r1b protein (purple) was labeled in BLA. The AP distance from bregma is given (in millimeters). Scale bars, 250 μm.

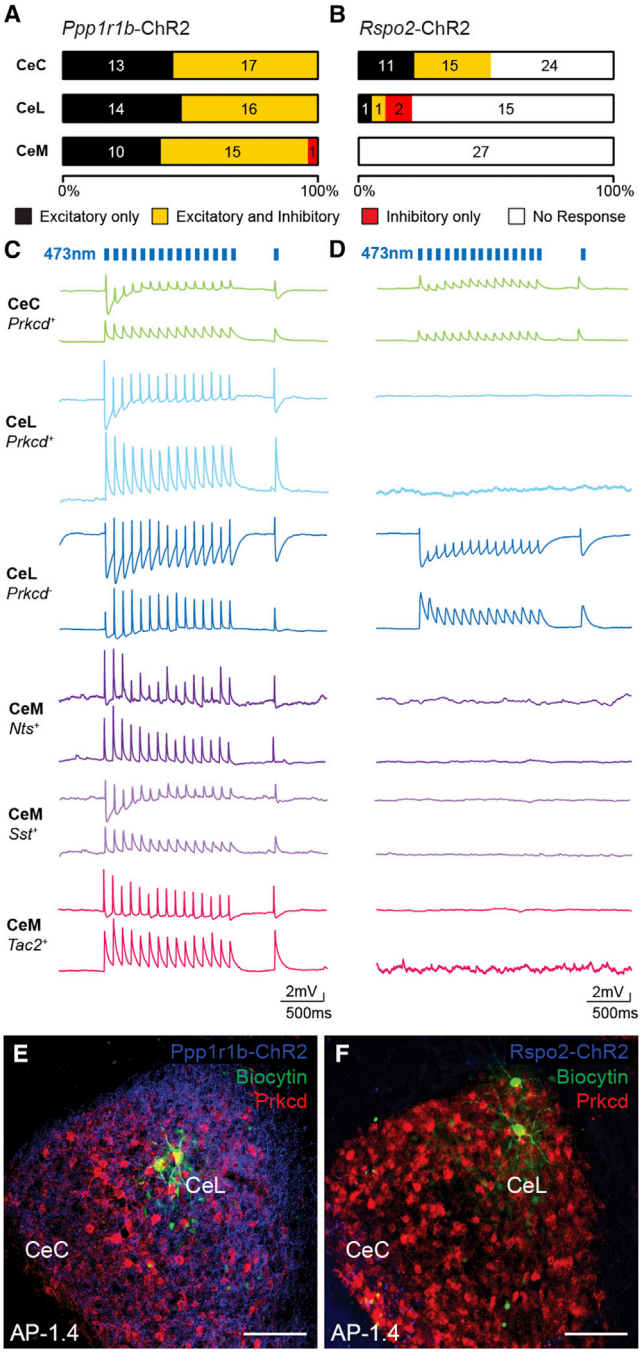

Figure 6. BLA *Ppp1r1rb*$^+$ and *Rspo2*$^+$ Neurons Make Monosynaptic Excitatory and Disynaptic Inhibitory Connections to Distinct CeA Neurons

(A and B) The proportion and number of CeC, CeL, and CeM neurons that receive only excitatory responses (black), both excitatory and inhibitory responses (yellow), only inhibitory responses (red), or no response (white) from blue-light stimulation of BLA *Ppp1r1b*-ChR2 fibers (A) or BLA *Rspo2*-ChR2 fibers (B). Numbers inside bars represent total number of neurons for each case.

(C and D) Example voltage-clamped traces of immunohistochemistry (IHC)- or qPCR-confirmed CeC *Prkcd*$^+$, CeL *Prkcd*$^+$, CeL *Prkcd*$^-$, CeM *Nts*$^+$, CeM *Sst*$^+$, and CeM *Tac2*$^+$ neurons in response to blue-light stimulation of BLA *Ppp1r1b*-ChR2 fibers (C) or BLA *Rspo2*-ChR2 fibers (D). Bottom traces represent responses at ~−70 mV, and top traces represent responses at ~−50 mV.

(E and F) Representative histology of IHC confirmation of CeL Prkcd$^+$ neurons in BLA *Ppp1r1b*-ChR2 slices (E) and CeL Prkcd$^-$ neurons in BLA *Rspo2*-ChR2 slices (F). The AP distance from bregma is given (in millimeters). Scale bars, 100 μm.

See also Figures S6J and S6K for counts of genetically confirmed neurons.

determined by latency (Figures S6F–S6I), in 100% of neurons in the CeC, 100% of neurons in the CeL, and 97% of neurons in the CeM. Among these neurons, disynaptic inhibition was also observed following monosynaptic excitation in 57% of neurons in the CeC, 53% of neurons in the CeL, and 60% of neurons in the CeM (Figure 6A). Connections with only disynaptic inhibition were observed in 3% of neurons in the CeM. Based on genetic-marker-based confirmation (Figures S6E and S6J), monosynaptic excitatory connections were observed in CeC *Prkcd*$^+$, CeL *Prkcd*$^+$, CeM *Nts*$^+$, CeM *Sst*$^+$, and CeM *Tac2*$^+$ neurons (Figures 6C and S6J). Blue-light stimulation in *Rspo2*-ChR2 slices resulted in monosynaptic excitation in 52% of neurons in the CeC, 11% of neurons in the CeL, and 0% of neurons in the CeM. Among these neurons, disynaptic inhibition following monosynaptic excitation was observed in 58% of neurons in the CeC and 50% of neurons in the CeL. Connections with only disynaptic inhibition were observed in 11% of CeL neurons (Figure 6B). Based on genetic-marker-based confirmation (Figures S6E and S6K), monosynaptic excitatory connections were observed in CeC *Prkcd*$^+$ neurons as well as in a CeL *Prkcd*$^-$ neuron (Figures 6D and S6K). These results show that BLA *Rspo2*$^+$ neurons mainly innervate CeC *Prkcd*$^+$ neurons, while making minimal connections to the CeL and CeM. In contrast, BLA *Ppp1r1b*$^+$ neurons innervate CeC *Prkcd*$^+$, CeL *Prkcd*$^+$, CeM *Nts*$^+$, CeM *Sst*$^+$, and CeM *Tac2*$^+$ neurons. In addition, 100% connectivity from BLA *Ppp1r1b*$^+$ neurons to CeL neurons suggests that BLA *Ppp1r1b*$^+$ neurons also innervate CeL *Sst*$^+$ and CeL *Crh*$^+$*Nts*$^+$*Tac2*$^+$. Although the identity of the neurons that mediate the polysynaptic inhibitory responses cannot be identified from these experiments, these functional experiments confirm the results of the rabies tracing experiments (Figure 5) and connectivity model of the BLA-to-CeA connectivity (Figure 8A).

The Appetitive and Aversive BLA-to-CeA Projections Are Analogous to Cortical Projections to Striatial Direct- and Indirect-Pathway Neurons

The BLA and CeA are cytoarchitecturally similar to the cortex and striatum, respectively (Carlsen and Heimer, 1988; Swanson and Petrovich, 1998). In the cortex, the direct pathway promotes movement and is characterized by intratelencephalic-type (IT-type) cortical neurons innervating dopamine receptor 1$^+$ (*Drd1*$^+$), dynorphin$^+$ (*Pdyn*$^+$), and substance P$^+$ (*Tac1*$^+$) striatonigral medium spiny neurons. The indirect pathway inhibits movement and is characterized by pyramidal tract-type (PT-type) neurons innervating dopamine receptor 2$^+$ (*Drd2*$^+$) and enkephalin$^+$ (*Penk*$^+$) striatopallidal medium spiny neurons (Gerfen et al., 1990; Reiner et al., 2010; Shepherd, 2013; Smith et al., 1998). Therefore, the expression of *Drd1*, *Drd2*, *Pdyn*, *Penk*, and *Tac1* was examined in the CeA to examine how the

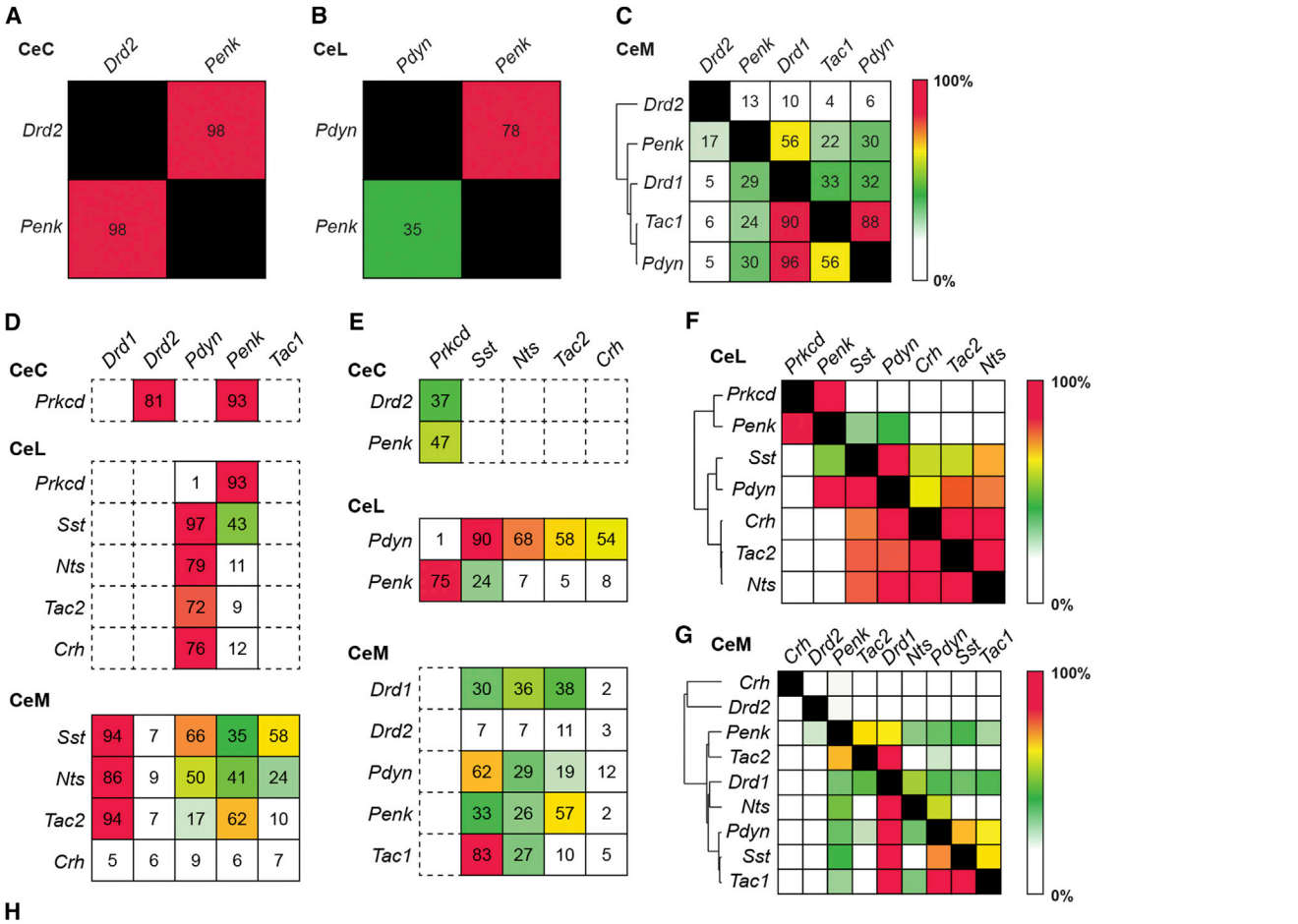

(legend on next page)

BLA-to-CeA circuit is organized compared to the direct and indirect pathways of the cortex and striatum. *Drd2* and *Penk* were expressed in the CeC. *Pdyn* and *Penk* were expressed in the CeL. *Drd1*, *Drd2*, *Pdyn*, *Penk*, and *Tac1* were expressed in the CeM (Figures S7A and S7B). Overlap of the expression of these striatal markers was examined in the CeA (Figures 7A, 7B, and S7C). In the CeC, *Penk* and *Drd2* were highly (>90%) overlapping (Figure 7A). In the CeL, *Penk* labeled 78% of *Pdyn*$^+$ neurons, while *Pdyn* labeled 35% of *Penk*$^+$ neurons (Figure 7B). In the CeM, hierarchical clustering using overlaps of the genes showed two major clusters. The first was *Drd2*, which minimally overlapped (<15%) with the other markers. The second contained *Drd1*, *Pdyn*, and *Penk*, which all moderately overlapped with one another (~30%–60%) except for *Pdyn*$^+$ neurons, with which most or all (>90%) coexpressed *Drd1* (Figure 7C). Using these sets of striatal markers, seven or eight genetically and regionally distinct populations can be identified. It should be noted that *Drd2* expression in the CeM is questionable. Though *Drd2* is expressed within the bounds of the CeM, its sparseness and expression pattern may reflect expression in the ventromedial extent of the CeC rather than the CeM. Further assessment using CTB retrograde tracing from the PAG resulted in no detectable CTB$^+$ neurons that were *Drd2*$^+$ (data not shown). Thus, like CeC neurons, *Drd2*$^+$ neurons likely do not project to the PAG; therefore, these CeM *Drd2*$^+$ neurons may reflect CeC *Drd2*$^+$ neurons.

The relationship between striatal markers and the CeA markers that were behaviorally and functionally characterized was examined using smFISH (Figures 7D–7H). In the CeC, *Drd2* and *Penk* were coexpressed in the majority (>80%) of *Prkcd*$^+$ neurons (Figure 7D), while *Prkcd* was coexpressed in a subset (~40%) of *Drd2*$^+$ and *Penk*$^+$ neurons (Figure 7E). In the CeL, *Penk* labeled the vast majority (>90%) of *Prkcd*$^+$ neurons and a subpopulation of *Sst*$^+$ neurons. *Pdyn* labeled virtually all (97%) of the *Sst*$^+$ neurons and the majority (70%–80%) of *Nts*$^+$, *Tac2*$^+$, and *Crh*$^+$ neurons (Figure 7D). In the CeL, hierarchical clustering using overlaps between all the genes revealed three major clusters: the first containing *Penk* and *Prkcd*; the second containing *Pdyn* and *Sst*; and the third containing *Crh*, *Nts*, and *Tac2* (Figure 7F). In the CeM, *Drd1* was coexpressed in the majority (>85%) of *Nts*$^+$, *Sst*$^+$, and *Tac2*$^+$ neurons. *Pdyn* and *Penk* were expressed in a subpopulation of *Nts*$^+$, *Sst*$^+$, and *Tac2*$^+$ neurons, with slightly more expression of *Pdyn* in *Sst*$^+$ neurons and more expression of *Penk* in *Tac2*$^+$ neurons (Figure 7D). In the CeM, hierarchical clustering using overlaps between all the genes revealed two major clusters: the first containing *Drd2* and the second containing *Drd1*, which can be further clustered into three groups—*Penk* and *Tac2*; *Drd1* and *Nts*; and *Pdyn*, *Sst,* and *Tac1* (Figure 7G). Results of gene expression in the CeA were summarized in a model (Figure 8B). These results show that CeC *Prkcd*$^+$ neurons express the striatal markers for the corticostriatal indirect pathway, *Drd2* and *Penk*, while CeM *Nts*$^+$, CeM *Sst*$^+$, and CeM *Tac2*$^+$ neurons mainly express the striatal markers for the corticostriatal direct pathway, *Drd1*, *Pdyn*, and *Tac1* (Gerfen et al., 1990; Smith et al., 1998).

DISCUSSION

Here, we identified a set of CeA neurons that are positive mediators for appetitive behaviors—CeL *Sst*$^+$, CeL *Crh*$^+$*Nts*$^+$*Tac2*$^+$, CeM *Nts*$^+$, CeM *Sst*$^+$, and CeM *Tac2*$^+$. These mediators of appetitive behavior receive monosynaptic input from BLA *Ppp1r1b*$^+$ neurons, while several of them also receive disynaptic input from BLA *Rspo2*$^+$ neurons. Given that BLA *Ppp1r1b*$^+$ neurons are capable of driving appetitive behaviors and that BLA *Rspo2*$^+$ neurons are capable of suppressing appetitive behaviors (Kim et al., 2016), these two pathways from the BLA to the CeA delineate an opposing circuit in the amygdala for the control of appetitive behaviors.

The CeA has an integral role in appetitive behaviors. The PAG has been shown to be a key site for executing defensive behaviors (Bandler and Depaulis, 1988; Kim et al., 1993), and several amygdala models hypothesized that the PAG-projecting CeA neurons mediate defensive behaviors (Duvarci and Pare, 2014; Fanselow, 1991; Herry and Johansen, 2014; Tovote et al., 2016). Although Cre transgenics and targeted virus injections would not necessarily give absolute selectivity when it comes to the functional study of neurons, none of the CeA neurons that were identified in this study and project to the PAG (Figures S5A–S5D)—CeL *Sst*$^+$, CeL *Crh*$^+$*Nts*$^+$*Tac2*$^+$, CeM *Nts*$^+$, CeM *Sst*$^+$, and CeM *Tac2*$^+$ neurons—elicit or are required for defensive behaviors or respond (using the expression of *Fos*) to stimuli that elicit defensive behaviors (Figures 2, 3, and 4). Rather, these PAG-projecting populations elicit appetitive behaviors (though not necessarily through their projections to the PAG) and were activated by stimuli that elicit or are associated with appetitive behaviors (Figures 2 and 3). Furthermore, although the global action of several of the genes (*Crh*, *Nts*, *Pdyn*, *Sst*, *Tac2*, and *Tac1*) that were found to be expressed in these PAG-projecting CeA neurons have been traditionally thought to be involved in negative behaviors and affective states, several studies that have

Figure 7. BLA-to-CeA Pathway for Appetitive Behavior Is Genetically Analogous to Corticostriatal Circuits

(A–C) Expression of striatal genetic markers in the CeA. Quantification of overlap of *Drd2* and *Penk* in the CeC (A). Quantification of overlap of *Pdyn* and *Penk* in the CeL (B). Quantification of overlap of *Drd2*, *Penk*, *Drd1*, *Tac1*, and *Pdyn* in the CeM (C). Values represent percent labeling of overlap of genes in column among genes in rows. For example, 35% of CeL *Penk*-labeled neurons coexpress *Pdyn* (B). Values represent percentage of labeling from totaling all cells counted from n = 3 mice. Hierarchical clustering was performed in the CeM using the percent overlap profile of each gene (C).

(D and E) Quantification of overlap of striatal markers—*Drd1*, *Drd2*, *Pdyn*, *Penk*, and *Tac1*—among *Prkcd*$^+$ neurons in the CeC; *Prkcd*$^+$, *Sst*$^+$, *Nts*$^+$, *Tac2*$^+$, and *Crh*$^+$ neurons in the CeL; and *Sst*$^+$, *Nts*$^+$, *Tac2*$^+$, and *Crh*$^+$ neurons in the CeM (D). Quantification of overlap of *Prkcd*, *Sst*, *Nts*, *Tac2*, and *Crh* among *Drd1*$^+$ and *Penk*$^+$ neurons in the CeC; *Pdyn*$^+$ and *Penk*$^+$ neurons in the CeL; and *Drd1*$^+$, *Drd2*$^+$, *Pdyn*$^+$, *Penk*$^+$ and *Tac1*$^+$ neurons in the CeM (E). Values represent percentage of labeling from totaling all cells counted from n = 3 mice.

(F and G) Overlap matrix of genes expressed in the CeL (F) and CeM (G). Values represent percentage of labeling from totaling all cells counted from n = 3 mice and include the percentage of labeling values found in Figure 1. Hierarchical clustering was performed from using the overlap profile of each gene.

(H) Representative histology of CeA expression of CeA genetic markers (*Prkcd*, *Sst*, *Nts*, *Tac2*, and *Crh*) with striatal markers (*Drd1*, *Drd2*, *Pdyn*, *Penk*, and *Tac1*). Scale bars, 50 μm.

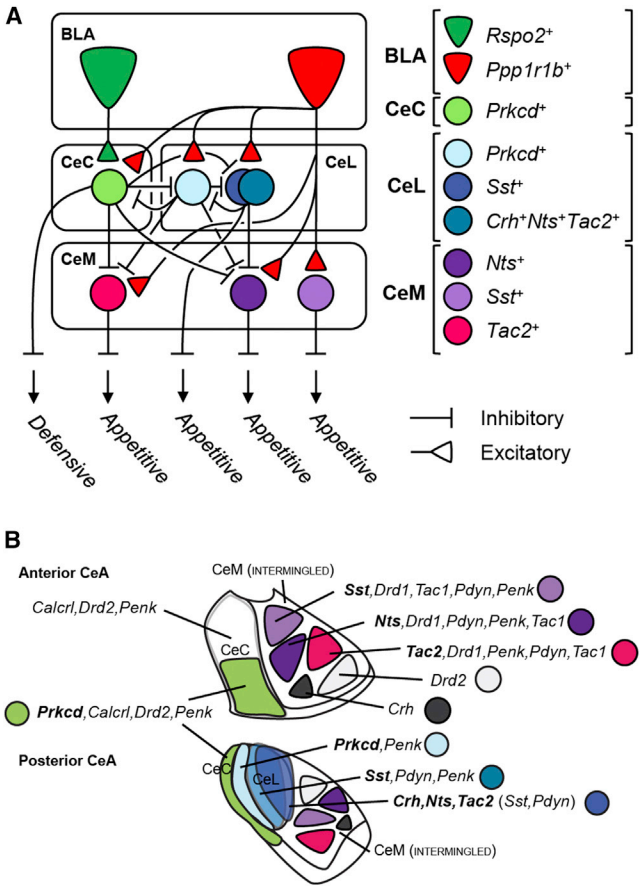

Figure 8. Summary of Anatomical and Genetic Results

(A) Structural and functional model of cell-type-specific BLA-to-CeA connectivity derived from monosynaptic rabies tracing experiments (Figures 2 and 5). BLA *Rspo2*$^+$ neurons mainly innervate CeC *Prkcd* neurons, which, in turn, innervate several CeA neurons that mediate appetitive behaviors. BLA *Ppp1r1b*$^+$ neurons innervate all CeA neurons in the model, CeA neurons that mediate appetitive behaviors as well as CeA *Prkcd*$^+$ neurons, which, in turn, innervate CeA neurons that mediate appetitive behaviors.

(B) Graphical summary of genetically distinct CeA populations and their spatial distribution within the CeA. CeM neurons (Figures 1 and 7), though not portrayed as intermingled, are intermingled. CeL neurons are overall intermingled but also have a slight spatial segregation as depicted in the cartoon.

examined the roles of these genes in the CeA and/or PAG have shown an opposing effect of these neuropeptides on negative behaviors or a positive role in appetitive behaviors, which is consistent with our findings (Bilkei-Gorzo et al., 2012; Cui et al., 2004; Helmchen et al., 1995; László et al., 2010; Merali et al., 1998; Rosén et al., 2004). Collectively, the populations that were examined in this study constitute almost all neurons (>90%) in the CeL and CeM, reinforcing the idea that the CeA participates in appetitive behaviors. Moreover, these data suggest that the main route for conveying defensive information from the BLA to the PAG may involve an alternative circuit that does not involve the CeL or CeM. Nevertheless, we do not disregard the role of the CeA in defensive behavior, as CeC *Prkcd*$^+$ neurons participate in defensive behaviors (Figures 2A and 4A). In addition, neither do we preclude the role of PAG-projecting CeA neurons in defensive or conditioned defensive behaviors, or the possibility of an unidentified neuronal population or a subpopulation of one of these populations for regulating defensive behaviors. However, in light of our findings and previous conflicting reports on the role of the CeA in defensive behavior (Cai et al., 2014; Koo et al., 2004; LeDoux et al., 1988; Li et al., 2013), further studies will be required to resolve how, if at all, defensive behaviors are positively mediated by the pathway from the CeA to the PAG. Nevertheless, the involvement of several distinct CeA projection neurons as positive mediators of appetitive behavior validates the integral role of the CeA in reward-related function (Badrinarayan et al., 2012; Gallagher and Chiba, 1996; Gallagher et al., 1990; Knapska et al., 2006; Parkinson et al., 2000; Ron and Barak, 2016).

CeC *Prkcd*$^+$ and CeL *Prkcd*$^+$ Neurons as Regulators of Defensive and Appetitive Behaviors

Studies on *Prkcd*$^+$ neurons in the CeA have suggested that there may be functional diversity among *Prkcd*$^+$ CeA neurons. An early study on *Prkcd*$^+$ neurons suggested a role in inhibition of defensive behavior (Haubensak et al., 2010). More recent studies have shown that CeA *Prkcd*$^+$ neurons inhibit feeding behavior (Cai et al., 2014) and that a subpopulation of *Prkcd*$^+$ neurons, CeA *Calcrl*$^+$ neurons, elicit and are required for defensive behavior (Han et al., 2015). Here, based on the gene expression pattern of *Calcrl* and *Prkcd*, *Calcrl*$^+$ neurons define neurons in the CeC (Figure S1B) (D'Hanis et al., 2007) rather than what was previously reported as the CeL in the study that described CeA *Calcrl*$^+$ neurons in defensive behaviors (Han et al., 2015). *Prkcd*$^+$ neurons reside in the CeL as well as define a subpopulation of *Calcrl*$^+$ neurons in CeC (Figure 1A) (Han et al., 2015). Considering this structural distinction, experiments between these two types of *Prkcd*$^+$ CeA neurons yielded behavioral, functional, and connectivity dissociations. CeC *Prkcd*$^+$ neurons elicit and are required for defensive behaviors and are activated by stimuli that drive defensive behaviors (Figures 2A and 3A). This is consistent with the reported role of CeA *Calcrl*$^+$ neurons in defensive behaviors (Han et al., 2015). In contrast, CeL *Prkcd*$^+$ neurons do not drive defensive behaviors but are activated by contextual fear extinction (Figures 2B and 3B). This is consistent with the initially hypothesized role of inhibition of defensive behaviors (Haubensak et al., 2010). Based on findings from retrograde rabies experiments, CeC *Prkcd*$^+$ and CeL *Prkcd*$^+$ are reciprocally connected (Figure 8A). Thus, *Prkcd*$^+$ neurons in the CeA represent two distinct populations that have opposing functions on defensive behavior, and we speculate that CeL *Prkcd*$^+$ neurons and CeC *Calcrl*$^+$ neurons, rather than CeL *Prkcd*$^+$ and CeL *Sst*$^+$ neurons (Duvarci and Pare, 2014; Herry and Johansen, 2014; Li et al., 2013), may represent the electrophysiological opposing units for fear-related responses in the CeA (Ciocchi et al., 2010; Haubensak et al., 2010).

With regard to appetitive behaviors, CeC *Prkcd*$^+$ and CeL *Prkcd*$^+$ neurons both directly inhibit mediators of appetitive behavior in the CeL and CeM (Figure 8A). Both *Prkcd*$^+$ populations are connected in such a way that they can support an inhibitory role on appetitive behaviors but may be functionally distinct based on differences in *Fos* activation profile and anatomical

inputs. CeC *Prkcd*$^+$ neurons are activated by threatening stimuli and aversive tastes (Figures 3A and 3D) and receive input from neurons that respond to aversive stimuli, BLA *Rspo2*$^+$ neurons (Figure 8A) and calcitonin-related polypeptide, alpha (*Calca*)-expressing neurons of the lateral parabrachial nucleus (by consideration that CeC *Prkcd*$^+$ neurons are a subpopulation of CeC *Calcrl*$^+$ neurons) (Carter et al., 2013; Han et al., 2015; Kim et al., 2016). In contrast, CeL *Prkcd*$^+$ neurons are activated by states of satiety (Cai et al., 2014) (Figure 3E) and receive input from BLA *Ppp1r1b*$^+$ neurons (Figure 8A), which respond to reward-related stimuli and *Calca*$^+$ neurons of the lateral parabrachial nucleus, which, in addition to responding to threat, also respond to states of satiety (Campos et al., 2016; Kim et al., 2016). Therefore, furthering previous findings and proposals on the role of CeA *Prkcd*$^+$ neurons (Cai et al., 2014), these results suggest that the role of CeC *Prkcd*$^+$ (and, by extension, CeC *Calcrl*$^+$) neurons is to signal the inhibition of appetitive behaviors mainly in response to aversive stimuli such as threat and aversive tastes, while the role of CeL *Prkcd*$^+$ neurons is to signal the inhibition of appetitive behaviors in response to positive states such as satiety.

CeL *Sst*$^+$ and CeL *Crh*$^+$*Nts*$^+$*Tac2*$^+$ Neurons as Positive Mediators for Drinking

CeL *Sst*$^+$ and CeL *Crh*$^+$*Nts*$^+$*Tac2*$^+$ neurons are *Prkcd*$^-$ neurons of the CeL. CeL *Prkcd*$^-$ neurons have been hypothesized to be positive mediators of fear-related behaviors (Duvarci and Pare, 2014; Herry and Johansen, 2014). A previous study has demonstrated that CeL *Sst*$^+$ neurons elicit and are required for defensive behaviors (Li et al., 2013). Contrary to these early findings, a more recent study suggested that activation of CeL *Prkcd*$^-$ neurons promotes feeding (Cai et al., 2014), while another study demonstrated that activation of CeL *Prkcd*$^-$ neurons suppresses defensive behaviors evoked by innate threatening odors (Isosaka et al., 2015). Here, we were unable to find evidence for CeL *Sst*$^+$ or CeL *Crh*$^+$*Nts*$^+$*Tac2*$^+$ neurons as mediators of defensive behavior (Figures 2, 3, and 4). We speculate that the main differences in our results from the original work on CeL *Sst*$^+$ neurons in defensive behaviors is likely attributed to our use of a lower volume of virus, 100 nL $\sim10^{12}$ versus 300 to 800 nL $\sim10^{12}$ viral particles, resulting in more specific targeting of the CeL (Li et al., 2013). Although a disinhibitory pathway that supports defensive behaviors from BLA *Rspo2*$^+$ neurons (positive mediators of defensive behaviors) to CeL *Prkcd*$^-$ neurons is anatomically identifiable (BLA *Rspo2*$^+$ to CeC *Prkcd*$^+$ to CeL *Prkcd*$^+$ to CeL *Prkcd*$^-$), a disynaptic inhibitory connection is also identifiable from BLA *Rspo2*$^+$ neurons, through CeC *Prkcd*$^+$ neurons to CeL *Prkcd*$^-$ neurons, which does not support defensive behaviors (Figure 8A). Moreover, CeL *Prkcd*$^-$ neurons receive direct innervation from BLA *Ppp1r1b*$^+$ neurons (Figure 8A), which suppress defensive behaviors and elicit appetitive behaviors (Kim et al., 2016). Thus, the anatomical and functional connectivity of *Prkcd*$^-$ neurons in relation to BLA neurons does not fully support a positive role in defensive behavior.

With regard to appetitive behaviors, CeL *Sst*$^+$ and CeL *Crh*$^+$*Nts*$^+$*Tac2*$^+$ neurons are capable of eliciting appetitive behaviors, are critical for drinking, and are strongly activated by water in addition to food (Figures 2C, 2D, 3D, 4C, and 4D). Moreover, inhibition of CeL *Prkcd*$^+$ neurons, which are reciprocally connected to CeL *Prkcd*$^-$ neurons, results in the enhancement of drinking behavior (Figure 4B), and a previous study demonstrated that activation of CeL *Prkcd*$^+$ neurons suppresses drinking behavior (Cai et al., 2014). Together, these results indicate that CeL *Sst*$^+$ and CeL *Crh*$^+$*Nts*$^+$*Tac2*$^+$ neurons are positive mediators of appetitive behavior and mainly participate in drinking-related function. These results bring insight to previous studies that have implicated the CeL in drinking- and alcohol-related behaviors (Dalmasso et al., 2015; Hwang et al., 2004; Kissler et al., 2014; Nie et al., 2004; Pereira-Derderian et al., 2010). With regard to the function of the two types of *Prkcd*$^-$ neurons, examination of CeL *Sst*$^+$ and CeL *Crh*$^+$*Nts*$^+$*Tac2*$^+$ neurons revealed no functional, behavioral, or connectivity differences. CeL *Sst*$^+$ and CeL *Crh*$^+$*Nts*$^+$*Tac2*$^+$ are highly overlapping populations: ~50% of CeL *Sst*$^+$ neurons are CeL *Crh*$^+$*Nts*$^+$*Tac2*$^+$, and ~70% of CeL *Crh*$^+$*Nts*$^+$*Tac2*$^+$ neurons are CeL *Sst*$^+$ (Figure 1B). Therefore, it was not unexpected that a structural or functional dissociation was not found.

CeM *Nts*$^+$, *Sst*$^+$, and *Tac2*$^+$ Neurons as Positive Mediators for Appetitive Behaviors

Genetically distinct CeM populations—*Nts*$^+$, *Sst*$^+$, *Tac2*$^+$—were found to participate in appetitive behaviors. Though gene expression of striatal markers in the CeM suggests that there may be alternative ways to divide CeM populations, these markers define three major well-segregated *Drd1*$^+$ neurons (Figures 1C and 7D). Behaviorally, these populations elicit appetitive behaviors, and collective silencing of these neurons results in reduced feeding and drinking (Figure S4). This is in contrast to CeL mediators of appetitive behavior, which appear to have a specific role in appetitive drinking behavior. Therefore, CeM neurons may have a more general role in appetitive behaviors. Alternatively, but not exclusively, the mediators of appetitive behavior in the CeL and CeM may function together to execute and regulate distinct behavioral programs for different types of appetitive behaviors and reward-related states. Although we did not assess the nuances of the different aspects of appetitive behaviors and reward-related phenotypes (Berridge and Robinson, 2003) or evaluate more long-term effects of silencing these neurons, further studies will be required to further dissociate the role of these distinct populations in appetitive behaviors.

Direct and Indirect Pathways of the Amygdala for Appetitive Behavior

The BLA-to-CeA circuit that promotes and suppresses appetitive behaviors is analogous to the cortex and striatum of the direct and indirect pathways of the basal ganglia that promotes and suppresses movement (Smith et al., 1998). CeM mediators of appetitive behavior express *Drd1*, *Pdyn*, and *Tac1* (Figure 7D). Although *Penk* is expressed in a subset of CeM mediators of appetitive behavior, *Drd2* is only minimally expressed (Figure 7D). CeM mediators of appetitive behavior directly receive monosynaptic input from excitatory *Ppp1r1b*$^+$ parvocellular neurons of the BLA (Figure 8A), which are also capable of promoting appetitive behaviors (Kim et al., 2016). Hence, the pathway for promoting appetitive behaviors from the BLA to the CeA is genetically and structurally analogous to cortex and striatum of the direct

pathway, which involves the direct innervation of *Drd1*$^+$, *Pdyn*$^+$, and *Tac1*$^+$ striatonigral neurons from excitatory IT-type neurons of the cortex (Gerfen et al., 1990; Reiner et al., 2010; Shepherd, 2013; Smith et al., 1998). The BLA-to-CeA pathway that supports the suppression of appetitive behavior emanates from BLA *Rspo2*$^+$ neurons and also may involve a subset of BLA *Ppp1r1b*$^+$ neurons in consideration of the connection from BLA *Ppp1r1b*$^+$ to CeA *Prkcd*$^+$ neurons (Figure 8A). Although BLA *Rspo2*$^+$ neurons are capable of driving defensive behaviors, they are also capable of suppressing appetitive behaviors (Kim et al., 2016) and form disynaptic inhibitory connections to mediators of appetitive behavior in the CeM and CeL (Figure 8A). The pathway from BLA *Rspo2*$^+$ neurons to CeA mediators of appetitive behavior involves an intermediate step in the CeC that express *Drd2* and *Penk* but does not express *Drd1*, *Pdyn*, or *Tac1* (Figure 7D). Hence, the pathway for suppressing appetitive behaviors, from excitatory *Rspo2*$^+$ magnocellular neurons of the BLA to the CeA, is functionally and genetically analogous to the cortex and striatum of the indirect pathway, which involves the direct innervation of *Drd2*$^+$ and *Penk*$^+$ striatopallidal neurons from PT-type neurons of the cortex (Gerfen et al., 1990; Reiner et al., 2010; Shepherd, 2013; Smith et al., 1998). Interestingly, the IT-type cortical neurons (direct pathway) are smaller in soma size than PT-type cortical neurons (indirect pathway) (Reiner et al., 2003), while BLA *Ppp1r1b*$^+$ parvocellular neurons are smaller in soma size than BLA *Rpso2*$^+$ magnocellular neurons (Kim et al., 2016). This suggests that the two types of BLA neurons may also be morphologically analogous to the two types of corticostriatal neurons. Although an analogy can be described between the BLA and CeA with the cortex and striatum, the output structures and circuitry of the CeA were not fully examined in this study. Thus, future studies will be required to examine whether the output of the CeA shares any organizing principle with the output circuitry of the striatum of the direct and indirect pathways.

Overall, the dissection of the connectivity from the BLA to the CeA and examination of the expression of striatal genetic markers in the CeA revealed corticostrial-like direct and indirect pathways between the BLA and CeA for the promotion and suppression of appetitive behaviors. The duplication and then specialization of structure and function is a common paradigm found in development and evolution. In the brain, this type of phenomenon is apparent in the stereotypic laminar organization of neurons across the cortex and between the glomeruli of the olfactory bulb (Ramón y Cajal, 1995). The similarities in architecture, genetics, and connectivity between the BLA/CeA and the cortex/striatum suggest that such an organizing principle of duplication and specialization may have occurred to give rise to what may be considered a corticostriatal neural circuit motif in the amygdala for appetitive behaviors.

STAR★METHODS

Detailed methods are provided in the online version of this paper and include the following:

- KEY RESOURCES TABLE
- CONTACT FOR REAGENT AND RESOURCE SHARING
- EXPERIMENTAL MODEL AND SUBJECT DETAILS
- METHOD DETAILS
  - Single Molecule Fluorescent In Situ Hybridization
  - Immunohistochemistry
  - Cell Counting
  - Stereotaxic Surgeries
  - Optogenetic Activation Experiments
  - Fos Activation Experiments
  - Optogenetic Inhibition Experiments
  - Retrograde Rabies Tracing
  - Optogenetic Slice Electrophysiology
  - Single Cell qPCR Genetic Confirmation
- QUANTIFICATION AND STATISTICAL ANALYSIS

SUPPLEMENTAL INFORMATION

Supplemental Information includes seven figures and can be found with this article online at http://dx.doi.org/10.1016/j.neuron.2017.02.034.

A video abstract is available at http://dx.doi.org/10.1016/j.neuron.2017.02.034#mmc3.

AUTHOR CONTRIBUTIONS

Conceptualization, J.K. and S.T.; Methodology, J.K. and X.Z.; Investigation, J.K., X.Z., and S.M.; Writing – Original Draft, J.K.; Writing – Review & Editing, J.K., S.M., X.Z, and S.T.; Resources, J.K., X.Z., S.M., and S.A.L.; Visualization, J.K.; Supervision, J.K. and S.T.; Funding Acquisition, S.T.

ACKNOWLEDGMENTS

We thank Akiko Wagatsuma for designing the operant behavioral chamber. We thank Ian Wickersham for providing the reagents for retrograde rabies tracing. We thank Christopher J. MacDonald and Teru Okuyama for reviewing the manuscript. This work is supported in part by NIH Pre-Doctoral Training Grant T32GM007287 (to J.K.) and by the RIKEN Brain Science Institute, the Howard Hughes Medical Institute, and the JPB Foundation (to S.T.).

Received: December 29, 2016
Revised: January 30, 2017
Accepted: February 15, 2017
Published: March 22, 2017

REFERENCES

Andero, R., Dias, B.G., and Ressler, K.J. (2014). A role for Tac2, NkB, and Nk3 receptor in normal and dysregulated fear memory consolidation. Neuron *83*, 444–454.

Badrinarayan, A., Prater, K.E., and Orsini, C.A. (2012). The role of the central amygdala in selecting circuits and responses. J. Neurosci. *32*, 8431–8433.

Bandler, R., and Depaulis, A. (1988). Elicitation of intraspecific defence reactions in the rat from midbrain periaqueductal grey by microinjection of kainic acid, without neurotoxic effects. Neurosci. Lett. *88*, 291–296.

Berridge, K.C., and Robinson, T.E. (2003). Parsing reward. Trends Neurosci. *26*, 507–513.

Bilkei-Gorzo, A., Erk, S., Schürmann, B., Mauer, D., Michel, K., Boecker, H., Scheef, L., Walter, H., and Zimmer, A. (2012). Dynorphins regulate fear memory: from mice to men. J. Neurosci. *32*, 9335–9343.

Cai, H., Haubensak, W., Anthony, T.E., and Anderson, D.J. (2014). Central amygdala PKC-δ(+) neurons mediate the influence of multiple anorexigenic signals. Nat. Neurosci. *17*, 1240–1248.

Campos, C.A., Bowen, A.J., Schwartz, M.W., and Palmiter, R.D. (2016). Parabrachial CGRP neurons control meal termination. Cell Metab. *23*, 811–820.

Carlsen, J., and Heimer, L. (1988). The basolateral amygdaloid complex as a cortical-like structure. Brain Res. *441*, 377–380.

Carter, M.E., Soden, M.E., Zweifel, L.S., and Palmiter, R.D. (2013). Genetic identification of a neural circuit that suppresses appetite. Nature *503*, 111–114.

Ciocchi, S., Herry, C., Grenier, F., Wolff, S.B.E., Letzkus, J.J., Vlachos, I., Ehrlich, I., Sprengel, R., Deisseroth, K., Stadler, M.B., et al. (2010). Encoding of conditioned fear in central amygdala inhibitory circuits. Nature *468*, 277–282.

Cornea-Hébert, V., Riad, M., Wu, C., Singh, S.K., and Descarries, L. (1999). Cellular and subcellular distribution of the serotonin 5-HT2A receptor in the central nervous system of adult rat. J. Comp. Neurol. *409*, 187–209.

Cui, X.Y., Lundeberg, T., and Yu, L.C. (2004). Role of corticotropin-releasing factor and its receptor in nociceptive modulation in the central nucleus of amygdala in rats. Brain Res. *995*, 23–28.

D'Hanis, W., Linke, R., and Yilmazer-Hanke, D.M. (2007). Topography of thalamic and parabrachial calcitonin gene-related peptide (CGRP) immunoreactive neurons projecting to subnuclei of the amygdala and extended amygdala. J. Comp. Neurol. *505*, 268–291.

Dalmasso, C., Antunes-Rodrigues, J., Vivas, L., and De Luca, L.A., Jr. (2015). Mapping brain Fos immunoreactivity in response to water deprivation and partial rehydration: Influence of sodium intake. Physiol. Behav. *151*, 494–501.

Davis, M. (1992). The role of the amygdala in fear and anxiety. Annu. Rev. Neurosci. *15*, 353–375.

Dubner, R., and Ruda, M.A. (1992). Activity-dependent neuronal plasticity following tissue injury and inflammation. Trends Neurosci. *15*, 96–103.

Duvarci, S., and Pare, D. (2014). Amygdala microcircuits controlling learned fear. Neuron *82*, 966–980.

Ehrlich, I., Humeau, Y., Grenier, F., Ciocchi, S., Herry, C., and Lüthi, A. (2009). Amygdala inhibitory circuits and the control of fear memory. Neuron *62*, 757–771.

Fanselow, M.S. (1991). The midbrain periaqueductal gray as a coordinator of action in response to fear and anxiety. In The Midbrain Periaqueductal Gray Matter: Functional, Anatomical and Neurochemical Organization (Vol. 213 of the NATO ASI Series), A. Depaulis and R. Bandler, eds. (Plenum Press), pp. 151–173.

Galaverna, O.G., Seeley, R.J., Berridge, K.C., Grill, H.J., Epstein, A.N., and Schulkin, J. (1993). Lesions of the central nucleus of the amygdala. I: Effects on taste reactivity, taste aversion learning and sodium appetite. Behav. Brain Res. *59*, 11–17.

Gallagher, M., and Chiba, A.A. (1996). The amygdala and emotion. Curr. Opin. Neurobiol. *6*, 221–227.

Gallagher, M., Graham, P.W., and Holland, P.C. (1990). The amygdala central nucleus and appetitive Pavlovian conditioning: lesions impair one class of conditioned behavior. J. Neurosci. *10*, 1906–1911.

Gerfen, C.R., Engber, T.M., Mahan, L.C., Susel, Z., Chase, T.N., Monsma, F.J., Jr., and Sibley, D.R. (1990). D1 and D2 dopamine receptor-regulated gene expression of striatonigral and striatopallidal neurons. Science *250*, 1429–1432.

Goosens, K.A., and Maren, S. (2001). Contextual and auditory fear conditioning are mediated by the lateral, basal, and central amygdaloid nuclei in rats. Learn. Mem. *8*, 148–155.

Han, S., Soleiman, M.T., Soden, M.E., Zweifel, L.S., and Palmiter, R.D. (2015). Elucidating an affective pain circuit that creates a threat memory. Cell *162*, 363–374.

Haubensak, W., Kunwar, P.S., Cai, H., Ciocchi, S., Wall, N.R., Ponnusamy, R., Biag, J., Dong, H.W., Deisseroth, K., Callaway, E.M., et al. (2010). Genetic dissection of an amygdala microcircuit that gates conditioned fear. Nature *468*, 270–276.

Helmchen, C., Fu, Q.G., and Sandkühler, J. (1995). Inhibition of spinal nociceptive neurons by microinjections of somatostatin into the nucleus raphe magnus and the midbrain periaqueductal gray of the anesthetized cat. Neurosci. Lett. *187*, 137–141.

Hemmings, H.C., Jr., Greengard, P., Tung, H.Y., and Cohen, P. (1984). DARPP-32, a dopamine-regulated neuronal phosphoprotein, is a potent inhibitor of protein phosphatase-1. Nature *310*, 503–505.

Herry, C., and Johansen, J.P. (2014). Encoding of fear learning and memory in distributed neuronal circuits. Nat. Neurosci. *17*, 1644–1654.

Hitchcock, J., and Davis, M. (1986). Lesions of the amygdala, but not of the cerebellum or red nucleus, block conditioned fear as measured with the potentiated startle paradigm. Behav. Neurosci. *100*, 11–22.

Hwang, B.H., Stewart, R., Zhang, J.K., Lumeng, L., and Li, T.K. (2004). Corticotropin-releasing factor gene expression is down-regulated in the central nucleus of the amygdala of alcohol-preferring rats which exhibit high anxiety: a comparison between rat lines selectively bred for high and low alcohol preference. Brain Res. *1026*, 143–150.

Isosaka, T., Matsuo, T., Yamaguchi, T., Funabiki, K., Nakanishi, S., Kobayakawa, R., and Kobayakawa, K. (2015). Htr2a-expressing cells in the central amygdala control the hierarchy between innate and learned fear. Cell *163*, 1153–1164.

Killcross, S., Robbins, T.W., and Everitt, B.J. (1997). Different types of fear-conditioned behaviour mediated by separate nuclei within amygdala. Nature *388*, 377–380.

Kim, J.J., Rison, R.A., and Fanselow, M.S. (1993). Effects of amygdala, hippocampus, and periaqueductal gray lesions on short- and long-term contextual fear. Behav. Neurosci. *107*, 1093–1098.

Kim, J., Pignatelli, M., Xu, S., Itohara, S., and Tonegawa, S. (2016). Antagonistic negative and positive neurons of the basolateral amygdala. Nat. Neurosci. *19*, 1636–1646.

Kissler, J.L., Sirohi, S., Reis, D.J., Jansen, H.T., Quock, R.M., Smith, D.G., and Walker, B.M. (2014). The one-two punch of alcoholism: role of central amygdala dynorphins/kappa-opioid receptors. Biol. Psychiatry *75*, 774–782.

Knapska, E., Walasek, G., Nikolaev, E., Neuhäusser-Wespy, F., Lipp, H.P., Kaczmarek, L., and Werka, T. (2006). Differential involvement of the central amygdala in appetitive versus aversive learning. Learn. Mem. *13*, 192–200.

Kohara, K., Pignatelli, M., Rivest, A.J., Jung, H.Y., Kitamura, T., Suh, J., Frank, D., Kajikawa, K., Mise, N., Obata, Y., et al. (2014). Cell type-specific genetic and optogenetic tools reveal hippocampal CA2 circuits. Nat. Neurosci. *17*, 269–279.

Koo, J.W., Han, J.S., and Kim, J.J. (2004). Selective neurotoxic lesions of basolateral and central nuclei of the amygdala produce differential effects on fear conditioning. J. Neurosci. *24*, 7654–7662.

László, K., Tóth, K., Kertes, E., Péczely, L., and Lénárd, L. (2010). The role of neurotensin in positive reinforcement in the rat central nucleus of amygdala. Behav. Brain Res. *208*, 430–435.

LeDoux, J.E., Iwata, J., Cicchetti, P., and Reis, D.J. (1988). Different projections of the central amygdaloid nucleus mediate autonomic and behavioral correlates of conditioned fear. J. Neurosci. *8*, 2517–2529.

Li, H., Penzo, M.A., Taniguchi, H., Kopec, C.D., Huang, Z.J., and Li, B. (2013). Experience-dependent modification of a central amygdala fear circuit. Nat. Neurosci. *16*, 332–339.

McCall, J.G., Al-Hasani, R., Siuda, E.R., Hong, D.Y., Norris, A.J., Ford, C.P., and Bruchas, M.R. (2015). CRH engagement of the locus coeruleus noradrenergic system mediates stress-induced anxiety. Neuron *87*, 605–620.

McDonald, A.J. (1984). Neuronal organization of the lateral and basolateral amygdaloid nuclei in the rat. J. Comp. Neurol. *222*, 589–606.

McDonald, A.J. (1991). Topographical organization of amygdaloid projections to the caudatoputamen, nucleus accumbens, and related striatal-like areas of the rat brain. Neuroscience *44*, 15–33.

Merali, Z., McIntosh, J., Kent, P., Michaud, D., and Anisman, H. (1998). Aversive and appetitive events evoke the release of corticotropin-releasing hormone and bombesin-like peptides at the central nucleus of the amygdala. J. Neurosci. *18*, 4758–4766.

Moga, M.M., and Gray, T.S. (1985). Evidence for corticotropin-releasing factor, neurotensin, and somatostatin in the neural pathway from the central nucleus of the amygdala to the parabrachial nucleus. J. Comp. Neurol. *241*, 275–284.

Nie, Z., Schweitzer, P., Roberts, A.J., Madamba, S.G., Moore, S.D., and Siggins, G.R. (2004). Ethanol augments GABAergic transmission in the central amygdala via CRF1 receptors. Science *303*, 1512–1514.

Parkinson, J.A., Robbins, T.W., and Everitt, B.J. (2000). Dissociable roles of the central and basolateral amygdala in appetitive emotional learning. Eur. J. Neurosci. *12*, 405–413.

Penzo, M.A., Robert, V., and Li, B. (2014). Fear conditioning potentiates synaptic transmission onto long-range projection neurons in the lateral subdivision of central amygdala. J. Neurosci. *34*, 2432–2437.

Pereira-Derderian, D.T.B., Vendramini, R.C., Menani, J.V., and De Luca, L.A., Jr. (2010). Water deprivation-induced sodium appetite and differential expression of encephalic c-Fos immunoreactivity in the spontaneously hypertensive rat. Am. J. Physiol. Regul. Integr. Comp. Physiol. *298*, R1298–R1309.

Pitkänen, A., Savander, V., and LeDoux, J.E. (1997). Organization of intra-amygdaloid circuitries in the rat: an emerging framework for understanding functions of the amygdala. Trends Neurosci. *20*, 517–523.

Pomrenze, M.B., Millan, E.Z., Hopf, F.W., Keiflin, R., Maiya, R., Blasio, A., Dadgar, J., Kharazia, V., De Guglielmo, G., Crawford, E., et al. (2015). A transgenic rat for investigating the anatomy and function of corticotrophin releasing factor circuits. Front. Neurosci. *9*, 487.

Ramón y Cajal, S. (1995). Histology of the Nervous System of Man and Vertebrates (New York: Oxford University Press).

Reiner, A., Jiao, Y., Del Mar, N., Laverghetta, A.V., and Lei, W.L. (2003). Differential morphology of pyramidal tract-type and intratelencephalically projecting-type corticostriatal neurons and their intrastriatal terminals in rats. J. Comp. Neurol. *457*, 420–440.

Reiner, A., Hart, N.M., Lei, W., and Deng, Y. (2010). Corticostriatal projection neurons - dichotomous types and dichotomous functions. Front. Neuroanat. *4*, 142.

Ritter, S., and Hutton, B. (1995). Mercaptoacetate-induced feeding is impaired by central nucleus of the amygdala lesions. Physiol. Behav. *58*, 1215–1220.

Robinson, M.J.F., Warlow, S.M., and Berridge, K.C. (2014). Optogenetic excitation of central amygdala amplifies and narrows incentive motivation to pursue one reward above another. J. Neurosci. *34*, 16567–16580.

Ron, D., and Barak, S. (2016). Molecular mechanisms underlying alcohol-drinking behaviours. Nat. Rev. Neurosci. *17*, 576–591.

Rosén, A., Zhang, Y.X., Lund, I., Lundeberg, T., and Yu, L.C. (2004). Substance P microinjected into the periaqueductal gray matter induces antinociception and is released following morphine administration. Brain Res. *1001*, 87–94.

Sanford, C.A., Soden, M.E., Baird, M.A., Miller, S.M., Schulkin, J., Palmiter, R.D., Clark, M., and Zweifel, L.S. (2017). A central amygdala CRF circuit facilitates learning about weak threats. Neuron *93*, 164–178.

Seo, D.O., Funderburk, S.C., Bhatti, D.L., Motard, L.E., Newbold, D., Girven, K.S., McCall, J.G., Krashes, M., Sparta, D.R., and Bruchas, M.R. (2016). A GABAergic projection from the centromedial nuclei of the amygdala to ventromedial prefrontal cortex modulates reward behavior. J. Neurosci. *36*, 10831–10842.

Shepherd, G.M. (2013). Corticostriatal connectivity and its role in disease. Nat. Rev. Neurosci. *14*, 278–291.

Skofitsch, G., and Jacobowitz, D.M. (1985). Calcitonin gene-related peptide: detailed immunohistochemical distribution in the central nervous system. Peptides *6*, 721–745.

Smith, Y., Bevan, M.D., Shink, E., and Bolam, J.P. (1998). Microcircuitry of the direct and indirect pathways of the basal ganglia. Neuroscience *86*, 353–387.

Swanson, L.W., and Petrovich, G.D. (1998). What is the amygdala? Trends Neurosci. *21*, 323–331.

Tovote, P., Esposito, M.S., Botta, P., Chaudun, F., Fadok, J.P., Markovic, M., Wolff, S.B., Ramakrishnan, C., Fenno, L., Deisseroth, K., et al. (2016). Midbrain circuits for defensive behaviour. Nature *534*, 206–212.

Warden, M.K., and Young, W.S., 3rd (1988). Distribution of cells containing mRNAs encoding substance P and neurokinin B in the rat central nervous system. J. Comp. Neurol. *272*, 90–113.

Wickersham, I.R., Lyon, D.C., Barnard, R.J., Mori, T., Finke, S., Conzelmann, K.K., Young, J.A., and Callaway, E.M. (2007). Monosynaptic restriction of transsynaptic tracing from single, genetically targeted neurons. Neuron *53*, 639–647.

Zirlinger, M., Kreiman, G., and Anderson, D.J. (2001). Amygdala-enriched genes identified by microarray technology are restricted to specific amygdaloid subnuclei. Proc. Natl. Acad. Sci. USA *98*, 5270–5275.

STAR★METHODS

KEY RESOURCES TABLE

Further information and requests for resources and reagents should be directed to and will be fulfilled by the Lead Contact Susumu Tonegawa (tonegawa@mit.edu)

REAGENT or RESOURCE	SOURCE	IDENTIFIER
Antibodies		
Rabbit monoclonal anti-PPP1R1B	Abcam	Cat#ab40801
Rabbit monoclonal anti-PKC-δ	Abcam	Cat#ab182126
Chicken polyclonal anti-Gfp	Invitrogen	Cat#A10262
Goat anti-rabbit Alexa Fluor 647	Invitrogen	Cat#A21244
Goat anti-chicken Alexa Fluor 488	Invitrogen	Cat#A11039
CF555 Streptavidin	Biotium	Cat#29038
Chemicals, Peptides, and Recombinant Proteins		
CCK Octapeptide, sulfated	Tocris	Cat#1166
Quinine hydrochloride dihydrate	Sigma	Cat#Q1125
Alexa Fluor 647-conjugated cholera toxin subunit B	Thermofisher	Cat#C34776
Critical Commercial Assays		
RNASCOPE Multiplex Fluorescent Assay	ACDBio	Cat#320851
TaqMan Gene Expression Assay	Thermofisher	Cat#4369016
SuperScript III CellsDirect cDNA Synthesis Kit	Thermofisher	Cat# 18080200
Experimental Models: Organisms/Strains		
Wild-type mice	JAX Laboratories	Stock #000664
Cartpt-Cre mice	GENSAT	Tg(Cartpt-cre)RY16Gsat/Mmucd
Crh-Cre mice	JAX Laboratories	B6(Cg)-Crh < tm1(cre)Zjh > /J
Drd1-Cre mice	JAX Laboratories	B6;129-Tg(Drd1a-cre)120Mxu/Mmjax
Nts-Cre mice	JAX Laboratories	B6;129-Nts < tm1(cre)Mgmj > /J
Prkcd-Cre mice	GENSAT	Tg(Prkcd-glc-1/CFP,-cre)EH124Gsat
Rspo2-Cre mice	In house	Kim et al., 2016
Sst-Cre mice	JAX Laboratories	Sst < tm2.1(cre)Zjh > /J
Tac2-Cre mice	JAX Laboratories	B6.129-Tac2 < tm1.1(cre)Qima > /J
Recombinant DNA		
AAV_9-Ef1a-DIO-ChR2	Upenn Vector Core	CS0633-3CS
AAV_9-Ef1a-DIO-eArch3.0	UNC Vector Core	Lot: AV5257
AAV_1-synP-FLEX-sTpEpB (Rabies helper virus)	Ian Wickersham	Kohara et al., 2014
SADΔG-mCherry (G-protein deleted rabies virus)	Ian Wickersham	Kohara et al., 2014
Sequence-Based Reagents		
RNAscope Probe Calcrl	ACDBio	Cat#452281
RNAscope Probe Crh	ACDBio	Cat#316091
RNAscope Probe Drd1	ACDBio	Cat#406491
RNAscope Probe Drd2	ACDBio	Cat#406501
RNAscope Probe Fos	ACDBio	Cat#421981
RNAscope Probe Gad1	ACDBio	Cat#400951
RNAscope Probe Htr2a	ACDBio	Cat#401291
RNAscope Probe Nts	ACDBio	Cat#420441
RNAscope Probe Pdyn	ACDBio	Cat#318771
RNAscope Probe Penk	ACDBio	Cat#318761
RNAscope Probe Prkcd	ACDBio	Cat#441791
RNAscope Probe Sst	ACDBio	Cat#404631

(*Continued on next page*)

Continued

REAGENT or RESOURCE	SOURCE	IDENTIFIER
RNAscope Probe Tac1	ACDBio	Cat#410351
RNAscope Probe Tac2	ACDBio	Cat#446391
Taqman Gene Expression Probe Prkcd	Thermofisher	Cat#Mm00440891_m1
Taqman Gene Expression Probe Sst	Thermofisher	Cat#Mm00436671_m1
Taqman Gene Expression Probe Nts	Thermofisher	Cat#Mm00481140_m1
Taqman Gene Expression Probe Tac2	Thermofisher	Cat#Mm01160362_m1
Software and Algorithms		
Solomon Coder	https://solomoncoder.com	
Video Freeze	Med Associates	SOF-843
Med-PC	Med Associates	SOF-735

CONTACT FOR REAGENT AND RESOURCE SHARING

Materials, datasets, and protocols are available upon request to the corresponding author, Susumu Tonegawa (tonegawa@mit.edu).

EXPERIMENTAL MODEL AND SUBJECT DETAILS

6- to 12-week-old male mice were used for all experiments, except 5- to 6-week-old male mice were used for slice patch clamp experiments. All Cre transgenic mice were bred using a heterozygous male with females of C57BL/6 background. *Crh*-Cre, *Drd1a*-Cre, *Rspo2*-Cre, *Sst*-Cre, and *Tac2*-Cre mice had a C57BL/6 background. *Cartpt*-Cre, *Nts*-Cre, and *Prkcd*-Cre mice were crossed to a C57BL/6 background for at least 2 generations from their original backgrounds from JAX laboratories or GENSAT. Cre-expressing mice were genetic knock-in mice or has been previously been validated for genetic specificity (Haubensak et al., 2010; Kim et al., 2016). BLA *Rspo2*$^+$ neurons were targeted using *Rspo2*-Cre mice. BLA *Ppp1r1b*$^+$ neurons were targeted using *Cartpt*-Cre mice (Kim et al., 2016). CeC *Prkcd*$^+$ and CeL *Prkcd*$^+$ neurons were targeted using *Prkcd*-Cre mice. CeL *Sst*$^+$ and CeM *Sst*$^+$ neurons were targeted using *Sst*-Cre mice. CeL *Crh*$^+$*Nts*$^+$*Tac2*$^+$ neurons were targeted using *Crh*-Cre mice. CeM *Nts*$^+$ neurons were targeted using *Nts*-cre mice. CeM *Tac2*$^+$ neurons were targeted using *Tac2*-Cre mice. CeM *Drd1*$^+$ neurons were targeted using *Drd1a*-Cre mice. Mice undergoing all behavioral tests (optogenetic experiments, *Fos* experiments) were single housed for 1 week prior to experiments and kept on a 12 hr light, 12 hr dark light cycle. Control mice for behavioral experiments underwent identical procedures as experimental mice, but were Cre$^-$ mice of the same sex from the same litters. Mice that underwent slice patch clamp experiments or rabies tracing experiments were grouped housed. All mice were maintained and cared in accordance with protocols approved by the Massachusetts Institute of Technology (MIT) Committee on Animal Care (CAC) and guidelines by the National Institutes of Health (NIH).

METHOD DETAILS

Single Molecule Fluorescent In Situ Hybridization

For examination of gene expression and *Fos* experiments, tissue samples underwent single molecule fluorescent *in situ* hybridization (smFISH). Isoflurane anesthetized mice were decapitated, brain harvested and flash frozen on aluminum foil on dry ice. Brains were stored at −80°C. Prior to sectioning, brains were equilibrated to −16°C in a cryostat for 30 min. Brains were cryostat sectioned coronally at 20 μm and thaw-mounted onto Superfrost Plus slides (25x75 mm, Fisherbrand). Sections from a single brain would be serially thaw-mounted onto 10 slides through the CeA, anterior-posterior distance from Bregma (−0.6 mm to −1.8 mm). Slides were air-dried for 60 to 90 min prior to storage at −80°C. smFISH for all genes examined—*Calcrl* (ACDBio Cat#452281), *Crh* (ACDBio Cat#316091), *Drd1* (ACDBio Cat#406491), *Drd2* (ACDBio Cat#406501), *Fos* (ACDBio Cat#421981), *Gad1* (ACDBio Cat#400951), *Htr2a* (ACDBio Cat#401291), *Nts* (ACDBio Cat#420441), *Pdyn* (ACDBio Cat#318771), *Penk* (ACDBio Cat#318761), *Prkcd* (ACDBio Cat#441791), *Sst* (ACDBio Cat#404631), *Tac1* (ACDBio Cat#410351), *Tac2* (ACDBio Cat#446391)—was performed using RNAscope Fluorescent Multipex Kit (Advanced Cell Diagnostics) as previously described (Kim et al., 2016). Slides were counterstained for the nuclear marker DAPI using ProLong Diamond Antifade mounting medium with DAPI (ThermosFisher).

Immunohistochemistry

For visualizing Prkcd, Ppp1r1b, Rabies helper virus expression (eGFP), ChR2-eYFP and ArchT-eYFP expression, tissue samples underwent immunohistochemistry (IHC). Mice were euthanized by avertin overdose and underwent a standard perfusion protocol using 1X phosphate-buffered saline (PBS), followed by 4% paraformaldehyde. Mouse brains removed and postfixed overnight at room temperature. Brains were vibratome sectioned at 50 μm and collected through the CeA, anterior-posterior distance from Bregma (−0.6 mm to −1.8 mm). IHC was performed as previously described (Kim et al., 2016) with primary antibodies anti-rabbit

PKC-δ (1:1000, Abcam Cat#ab18212), anti-rabbit PPP1R1B (1:1000, Abcam Cat# ab40801), chicken anti-GFP (Invitrogen Cat#A10262) and secondary antibodies Alexa Fluor 647-conjugated Goat anti-Rabbit (1:1000, Invitrogen Cat#A21244), Alexa Fluor 488-conjugated Goat anti-chicken (1:1000, Invitrogen Cat#A11039). In the slice patch clamp experiments, brain slices were fixed for 4 hr at 4°C prior to undergoing the IHC protocol (Kim et al., 2016), biocytin was labeled using CF555 Strepatvidin (1:100, Biotium Cat#29038) during the secondary antibody incubation step.

Cell Counting

Images of smFISH and retrograde rabies tracing experiments were taken using a standard fluorescent microscope (Zeiss) under a 10X objective. Colors represented in micrographs are false colors and do not necessarily reflect native colors. Images were exported and counted manually using cell counting software (ImageJ). Percent labeling found in Figures 1 and 7 were quantified by counting 1 to 3 sections equal number per mouse, from n = 3 mice and sum totaling all single and double labeled neurons to yield a raw percentage value. The bounds of what considered the CeC, CeL, and CeM were used as shown in cartoons in Figures S1B and S7B. Although CeC in the posterior portion of the CeA (anterior-posterior Bregma −1.6 mm) is depicted in Figures and defined by atlas boundaries lying laterally to the CeL, the posterior CeC was not quantified in any quantification of CeC neurons as the boundary between the CeC and CeL in the posterior CeA is ambiguous.

Stereotaxic Surgeries

Mice underwent standard stereotactic procedures under isoflurane anesthesia. Vectors were injected using a mineral oil filled glass micropipette attached to a 1 μL microsyringe. For optogenetic experiments of the CeA, 100nL of AAV_9-Ef1a-DIO-ChR2 or AAV_9-Ef1a-DIO-eArch3.0 was bilaterally injected into the CeC (distance from Bregma, AP-0.8 mm, ML ± 2.9 mm, DV-5.0 mm), CeL (AP-1.4 mm, ML ± 2.9 mm, DV-4.7 mm), or CeM (AP-0.8 mm, ML ± 2.8 mm, DV-5.0 mm) of the different CeA Cre mice. Both ChR2 and Arch viruses were diluted in 1X phosphate buffer (PBS, pH 7.2), one part stock virus, 3 parts PBS to give a final concentration of $\sim 1.0 \times 10^{12}$ GC. Subsequent to injections, 5.0 mm Mono fiberoptic cannulas (Doric Lens) were implanted above the site of injection of the CeC (DV-4.4 mm), CeL (DV-4.2 mm), or CeM (DV-4.4 mm). Once positioned above the CeA, the mono fiberoptic cannula was cemented using dental cement (Teets cold cure; A-M Systems) to the skull, which contained 2 screws that were posterior and medial to the injection site. Once the dental cement cured, a protective cap surrounding the implant, made using a 1.5mL black Eppendorf tube, was fixed onto the implant using dental cement. Post-operation, mice received an injection of slow release buprenorphine (1mg/kg). Mice spent 1 week for recovery and then were handled by investigator 2-3 days prior to behavioral experiments. For slice patch clamp experiments, 200nL of AAV_9-Ef1a-DIO-ChR2 was into the BLA of Rspo2-Cre (AP-1.3 mm, ML ± 3.3 mm, DV-4.85 mm) and Cartpt-Cre mice (AP-4.8 mm, ML ± 0.5 mm, DV-3.0 mm) and incubated for 1 week prior to sacrifice for the slice patch clamp experiments. For CTB retrograde tracing, Alexa Fluor 647-conjugated cholera toxin subunit B (1 μg/μL, Thermofischer Cat#C34778) was unilaterally injected into the PAG (300 nL, AP-1.0 mm, ML+2.9 mm, DV-4.5 mm). 1 week later, mice were sacrificed and brains underwent smFISH.

Optogenetic Activation Experiments

ChR2 virus-injected mice and Cre^- control mice underwent an optogenetic freezing test followed by an optogenetic self-stimulation test. These optogenetic activation experiments were performed on cohorts of 6 to 12 mice and took place during first half of the dark cycle. The optogenetic freezing test involved exposing mice to conditioning chamber (Med Associates) for 6 min. During the 0-3 min period, mice did not receive any optogenetic stimulation. During the 3-6 min period, mice received continuous optogenetic stimulation, 10-15-mW 20-Hz 473-nm light stimulation. 1 day later, mice were food deprived for 24 hr prior to the start of the optogenetic self-stimulation test. Videos were captured using Video Freeze software (Med Associates). The optogenetic self-stimulation test took place in an operant conditioning chamber (Med Associates) equipped with a two nose ports. Prior to the trial, one of the two nose ports was randomly assigned to deliver optogenetic stimulation, 5 s duration 10-15-mW 20-Hz 473-nm light stimulation, upon nose poke (ON port), while the other one did not deliver optogenetic stimulation (OFF). Each of the nose points contained a single food pellet to initiate the mouse into the port. Mice were then placed into the operant chamber for 60 min. For the optogenetic freezing test, freezing was scored as the duration of freezing as percentage of total time of the trail on day 2 and from the onset of the first shock to the end of the experiment on day 1. Freezing was scored manually and blind to the condition of the mouse using behavioral scoring software (Solomon Coder). For the optogenetic self-stimulation test, total numbers of pokes on the OFF and ON port were automatically counted and obtained through MED-PC (Med Associates) software. Mice where lack of or non-specific ChR2 expression or improper optic fiber placement occurred were removed from behavioral analysis. 9 out of 52 animals were removed from analysis blind to behavioral results (Figure 2).

Fos Activation Experiments

For all *Fos* staining, 6 hr prior to sacrifice, food and water were removed from the home cages of C57BL/6 wild-type mice in order to reduce any unintended activation in the *Fos* experiments. Mice were exposed to a fear conditioning chamber (Med Associates) for 500 s in which 3 footshocks (.75mA) were delivered at the 198 s, 278 s, 358 s time points, while control mice underwent the same procedure, but did not receive any footshocks. Mice were returned to their home cages and 30 min later sacrificed. Mice undergoing fear extinction underwent the same 3 shock fear conditioning protocol, then 24 hr later, were exposed to the fear conditioning chamber without any footshocks 3 times, for 15 min. Mice spent 1 hr in between these 3 15 min extinction sessions. 24 hr later, mice were

exposed to the fear conditioning chamber for 5 min, returned to their home cages, and sacrificed 30 min later. Control mice underwent similar procedures, but did not undergo the 3 15 min extinction sessions. Hence, control mice can be considered mice undergoing 48 hr contextual fear recall, rather than contextual fear extinction recall. 24 hr food-deprived mice were transported into an experimental room on a cart and then exposed to ad libitum food, in their home cages. After 30 min from the end of the first feeding bout, mice were sacrificed. Control mice underwent identical procedures but did not receive food. This involved carting the mice to the experimental room and opening the lid of their home cages. 24 hr water-deprived mice that were exposed to water in an analogous way food was presented to food-deprived mice. Quinine water exposed mice were given quinine water (.01% quinine, Sigma) rather than water, only mice that displayed aversion to quinine water (having drinking bouts that were less than 2-3 s) were sacrificed. Control mice underwent identical procedures but did not receive water. Mice were sacrificed 30 min after the exposure to the stimulus. Mice were given CCK injections (5 μg/kg of CCK dissolved in 0.9% sodium chloride saline solution, Tocris), while control mice received saline injections intraperitoneally within the first hour of the dark cycle. Mice were sacrificed 30 min after the injections. *Fos* expression in CeC *Prkcd*$^+$ and CeL *Prkcd*$^+$ neurons was examined using *Prkcd* (ACDBio, Cat#441791). *Fos* expression in CeL *Sst*$^+$ and CeM *Sst*$^+$ neurons was examined using *Sst* (ACDBio, Cat#404631). *Fos* expression in CeL *Crh*$^+$*Nts*$^+$*Tac2*$^+$ and CeM *Tac2*$^+$ neurons was examined using *Tac2* (ACDBio, Cat#446391). *Fos* expression in CeM *Nts*$^+$ neurons was examined using *Nts* (ACDBio, Cat#420441).

Optogenetic Inhibition Experiments

Arch virus-injected mice underwent a feeding test, followed by a drinking test, then followed by a contextual fear conditioning test. For the feeding test, mice were food-deprived for 24 hr prior to the start of the experiment, which took place during the first half of the dark cycle. For the feeding test, mice were exposed to ad libitum food in their home cages while receiving constant 10-15-mW 532-nm light inhibition for 20 min. After the feeding test, mice returned to their normal diet until the start of the light cycle (approximately 12 hr later) in which mice were water-deprived. Approximately 18 hr later, in the second half of the dark cycle, mice underwent the drinking test. In the drinking test, mice were exposed to ad libitum water for 5 min in a chamber identical to their home cages but without bedding. During the entirety of the 5 min drinking test, mice received constant 10-15-mW 532-nm light inhibition. After the test, mice were returned to their normal diet. The next day, mice underwent contextual fear conditioning. On day 1 of contextual fear conditioning, mice were placed into a fear conditioning chamber (Med Associates) for 500 s and received footshocks (.75mA) during the 198 s, 278 s, 358 s time points. Simultaneously with the onset of the footshock, a constant pulse of 532-nm light (10-15 mW) was delivered through the optical cannulas for duration of 30 s. On day 2, mice were returned to the fear conditioning chamber for 180 s, where no shock or laser was delivered. Feeding, drinking, and freezing were scored manually and blind to the condition of the mouse using behavioral scoring software (Solomon Coder). Behaviors were scored as a percentage, calculated by the duration of the time spend performing the behavior as a proportion of the behavioral trail time. Feeding was scored based on the mouse orally engaging food pellets (for instance, either actively chewing food or biting off small pieces of the larger food pellet) and drinking was scored based on the mouse orally contacting the water spout. Mice where lack of or non-specific Arch expression or improper optic fiber placement occurred were removed from behavioral analysis. 5 out of 137 animals were removed from analysis in a blind manner, prior to the scoring of behaviors (Figure 4 and Figure S4).

Retrograde Rabies Tracing

For monosynaptic retrograde rabies experiments, 100nL of rabies helper virus, AAV1-synP-FLEX-sTpEpB, was injected into the CeC, CeL, or CeM or CeA of Cre-expressing mice. 3 weeks later, 100nL EnvA G protein deleted rabies virus, SADΔG-mCherry, was injected into the same location. 1 week later, mice were sacrificed and brains underwent IHC using antibodies against PKC-δ (Abcam, Cat#ab182126) or PPP1R1B (Abcam, Cat#ab40801) and visualized using Alexa Fluor 647-conjugated secondary antibody (Invitrogen, Cat#A21244). Micrographs (Figure 5) of rabies experiment were adjusted so that all immunofluorescent cells signals are able to be visualized.

Optogenetic Slice Electrophysiology

Mice were anesthetized by isoflurane and their brains dissected. Using a vibratome (VT1000S, Leica), we prepared 300-μm-thick coronal slices containing the basolateral and central amygdala in oxygenated cutting solution at ~4°C. Slices were then incubated at ~23°C in oxygenated artificial cerebrospinal fluid (ACSF) for 45 min to a 1 hr. The cutting solution contained 3 mM KCl, 0.5 mM CaCl2, 10 mM MgCl2, 25 mM NaHCO3, 1.2 mM NaHPO4, 10 mM D-glucose, 230 mM sucrose, saturated with 95% O/5% CO (pH 7.3, osmolarity 340 mOsm). The ACSF contained 124 mM NaCl, 3 mM KCl, 2 mM CaCl2, 1.3 mM MgSO4, 25 mM NaHCO3, 1.2 mM NaHPO4, 10 mM D-glucose, saturated with 95% O/5% CO (pH 7.3, osmolarity 300 mOsm). Slices were transferred to a submerged experimental chamber and perfused with oxygenated 36°C ACSF at a rate of 3 mL min^{-1}.

Whole-cell recordings in current-clamp mode were performed using a patch clamp setup with an infrared differential interference contrast microscope (BX51, Olympus) with a water immersion 40 × objective (N.A. 0.8), four automatic micro-manipulators (Luigs & Neumann) and a CCD camera (Orca R2, Hamamatsu). Borosilicate glass pipettes were fabricated (P97, Sutter Instrument) with a resistances of 8–10 MΩ and filled with the following intracellular solution: 110 mM potassium gluconate, 10 mM KCl, 10 mM HEPES, 4 mM ATP, 0.3 mM GTP, 10 mM phosphocreatine and 0.5% biocytin (pH 7.25, osmolarity 290 mOsm). Biocytin was excluded from the intracellular solution if the cytosol of the patched neuron was aspirated for PCR. Access resistance was monitored throughout the duration of the experiment and data acquisition was suspended whenever the resting membrane potential was depolarized

above −50 mV or the access resistance was beyond 20 MΩ. Recordings were amplified using up to two dual-channel amplifiers (Multiclamp 700B, Molecular Devices), filtered at 2 kHz, digitized (20 kHz) and acquired using custom software running on Igor Pro (Wavemetrics). Software and code are available upon request. Gabazine was obtained from Tocris.

Optogenetic stimulation was achieved through a 460-nm LED light source (XLED1, Lumen Dynamics) driven by TTL input with a delay onset of 25 μs (subtracted offline). Light power on the sample was 33 mW mm−2, and only the maximum power was employed. Slices were stimulated by a train of 15 light pulses at 10 Hz repeated 20 times every 6 s. EPSPs, IPSPs and action potentials were measured at resting membrane potential of the patched cell.

The intrinsic electrophysiological properties were measured in current clamp mode with the cell held at −70 mV. Input resistance was estimated by linear fit of the I-V relationship (injection of 10–12 current steps of 1 s duration). Action potential threshold was tested with a current ramp injection. Synaptic connections were verified by taking an average of 10 to 20 individual trials from each patched neuron held at −55mV and −75mV. EPSP amplitude was measured from the average maximum peak response by subtracting a baseline obtained 5 ms before light pulse starts. EPSP onset was measured from the beginning of the light pulse to the starting point of the response. The first differential of the response wave was calculated and the first point of maximum change in voltage (y axis) was detected. The corresponding point in time (x axis) was noted. The difference between the two time points was determined to be the onset latency of the response. If a patched cell had only EPSPs at both −50 and −70mV holding potentials, the cell was determined to be excitatory only, putatively receiving only a direct fiber excitation. If a patched cell showed a combination of E and IPSPs at −50mV and EPSPs at −70mV, the cell was deemed to be excitatory and inhibitory, putatively receiving both direct glutamatergic excitation and the local interneuron generated feedforward inhibition. And finally, if the cell showed no EPSPs in response to light stimulation at both holding potentials, it was classified as inhibitory only. To compute the probability of connection (n successes/n tests) we used only slices with reliable ChR2 expression characterized at least by one responsive postsynaptic cell (principal cell or interneuron).

CeL neurons were filled with biocytin, slices were recovered and fixed in 4% paraformaldehyde for verification of genetic identify using IHC against Prkcd. Analysis for CeL Prkcd$^-$ neurons in addition ot CeL Prkcd$^+$ neurons was taken into consideration.

CeC and CeM neurons were harvested for subsequent qPCR analysis. In order to harvest the RNA of recorded neurons, a negative pressure of 250mbar was applied for 5 min followed by a stronger negative pressure of 500mbar also for 5 min. Successful suction of the cytosolic contents was visually confirmed by observing the patched cell shrink on the microscope screen. The negative pressure was maintained until the glass pipette was quickly withdrawn. It was then carefully lowered into a 0.2ml PCR tube until its tip was felt against the bottom of the tube. Finally, gentle positive pressure was applied to expel the contents on the pipette into a qPCR buffer solution (see below).

Single Cell qPCR Genetic Confirmation

Cytosolic harvests was quickly transferred to 0.2mL PCR tube fill with 10 μL RNase free water, 2 μL oligo(dT), 1 μL dNTP, 1 μL RNaseOUT provided by the SuperScript III CellsDirect cDNA Synthesis Kit (ThermoFisher). Samples were placed on a 70°C heat block for 5 min, and then chilled on ice. For first strand synthesis, 8 μL of RT mix was added to the sample (6 μL 5x RT Buffer, 1 μL 0.1M DTT, 1 μL Superscript III RT) and incubated on a 50°C heat block for 50 min. Next, the reverse transcriptase was inactivated by 10 min incubation on an 85°C heat block. Samples were stored in −20°C until quantitative polymerase chain reaction (qPCR).

qPCR was performed using the Taqman Gene Expression Assays (Thermofisher) for Prkcd in CeC neurons or for Nts, Sst, and Tac2 in CeM neurons. Each qPCR reaction consisted of 25 μL 2X TaqMan Gene Expression Master Mix, 7 μL of cDNA template, 17.5 μL of RNase free water, and 2.5 μL of the 20X TaqMan Gene Expression Assay of Prkcd (Cat#Mm00440891_m1), Nts (Cat#Mm00481140_m1), Sst (Cat#Mm00436671_m1), or Tac2 (Cat#Mm01160362_m1). qPCR reaction was performed in an Applied Biosystems 7500 Real-Time PCR System using the Fluorescein (FAM) channel with the standard qPCR reaction protocol for 60 cycles. Any positive amplification signal (ΔRn) within the 60 reaction cycles was considered to be positive confirmation for such gene. In contrast to IHC confirmation of CeL neurons, negative results from CeC and CeM qPCR confirmation was not considered because of the high levels of false negatives in qPCR amplification.

QUANTIFICATION AND STATISTICAL ANALYSIS

Data are represented as mean ± s.e.m.. All histograms display individual points, which represent the values and total number of individual samples. What the individual samples represent is indicated within the figure legends for all experiments. Student's *t test*, paired or unpaired wherever appropriate, was performed on all comparisons with exceptions being the one-way ANOVA with Bonferroni's correction between the comparison between water and quinine with no water groups (Figure 3D) and one-way ANOVA with Bonferroni's correction for multiple comparisons (Figures S6A and S6C). 95% confidence interval was used to determine significance. Significance was displayed as *$p < 0.05$, **$p < 0.01$, ***$p < 0.001$, ****$p > 0.0001$, not significant values were not denoted. Statistical tests were performed using GraphPad Prism 6.0. Hierarchical clustering was performed by generating a matrix containing the percent overlap profile of each gene in a given CeA subdivision, then calculating the distance using the pairwise distance function (pdist), dendrograms were made using the linkage function (linkage) on Matlab8.3. The diagonals on the percent labeling matrices corresponded to identical gene pairs. Therefore, for the cluster, the diagonals of the matrices were denoted as 100%.